REVIEW

Check for updates

State-of-the-art on the conversion of lignocellulosic biomass and its derivatives into biofuels using zeolites as catalysts

Odiri K. Siakpebru[ab] and Ana Rita C. Morais [ID] *[ab]

Lignocellulose is one of the most sustainable and renewable carbon sources for the production of biofuels. However, its complex and recalcitrant structure, typically composed of bulky and highly oxygenated molecules, results in significant challenges for catalytic conversion using zeolites as catalysts. These structural complexities often require multiple reaction steps and severe reaction conditions, making product selectivity, carbon recovery, and catalyst deactivation particularly relevant. This review provides the latest developments in the application of zeolites for the conversion of lignocellulosic biomass and its derivatives into biofuels. Both advantages and challenges associated with zeolites as well as the potential for further development of zeolites for the production of biofuels from lignocellulosic biomass feedstocks were discussed.

1. Introduction

The transportation industry accounts for 29% of global energy consumption.[1] In 2019, US commercial aviation was responsible for 2.5% of domestic and 11% of transportation sector GHG (greenhouse gas) emissions, respectively.[2] Although fossil

[a]Department of Chemical and Petroleum Engineering, University of Kansas, Lawrence, Kansas 66045, USA. E-mail: ana.morais@ku.edu

[b]Wonderful Institute for Sustainable Engineering, University of Kansas, Lawrence, Kansas, 66045, USA

fuels, such as oil, gas and coal, account for more than 80% of the total energy consumption,[3,4] their share is projected to decrease approximately 10% by 2040.[5] This projection accounts for the expected increase in heat and electricity production from solar, wind, hydroelectric and geothermal sources, as well as the increase in car fuel efficiency and emerging electric vehicle utilization.[6,7] In addition, according to BP Energy Outlook 2020, biofuels can play a major role in the aviation and marine transportation sectors.[3] While electricity and hydrogen can be used to decarbonize light-duty vehicles,[8–10] biomass is the only

Odiri Kingsley Siakpebru earned his bachelor's degree in chemical engineering from Nnamdi Azikiwe University, Awka, Nigeria, in 2007. He is presently a PhD candidate in Chemical and Petroleum Engineering at the University of Kansas, USA. Under the guidance of Dr Ana Morais, he is conducting research in the field of heterogeneous catalysis, focusing on the design, synthesis, and application of zeolite-based catalysts for the conversion of biomass into liquid hydrocarbons.

Odiri K. Siakpebru

Ana Rita C. Morais is an Assistant Professor of Chemical Engineering and the Deputy Director of the Wonderful Institute for Sustainable Engineering (WISE) at the University of Kansas. She earned her PhD in Sustainable Chemistry from NOVA University of Lisbon, Portugal, in 2018. In 2019, she joined the National Renewable Energy Laboratory to work on the catalytic conversion of lignin and the deconstruction of plastic waste. Her current research interests include using supercritical and subcritical fluids to deconstruct plastic waste, chemical conversion of waste biogenic feedstocks into sustainable aviation fuels and chemicals, and separation of high GWP refrigerant blends for recycling and upcycling.

Ana Rita C. Morais

renewable organic carbon source available in our planet that can be used to fuel airplanes and other heavy-duty transportation modes that are much less flexible in energy sources.[11] It is worth noting that the Sustainable Aviation Fuels (SAFs) Grand Challenge, involving USDA (US Department of Agriculture), DOT (Department of Transportation), and DOE (Department of Energy), was launched in 2021 and aims to supply 3 billion gallons of SAFs per year by 2030. The goal is to produce enough SAFs to fully meet the projected US aviation fuel demand of around 35 billion gallons per year by 2050.[2] According to the SAF Grand Challenge Roadmap, "(…) a continuous focus on supporting research, development, demonstration, and deployment of new feedstocks and conversion technologies (…)" is needed to achieve the latter goal. Also, the European Commission's 2020 ReFuelEU Aviation Initiative put forward the goal of achieving net-zero emissions in the European Union by 2050.[12]

Biofuels have the potential to significantly reduce reliance on petroleum-based gasoline and non-combustible fuels, provided that cost-effective, carbon-neutral technologies make it feasible to replace them with bio-based alternatives derived from biomass. Thus, a rapid transition from petroleum to price-competitive and low-carbon index drop-in transportation fuels to support long-term economic growth, energy security, and decrease in GHG emissions is a substantial endeavor of our world today.[13,14] Important advances have been made in the biomass-to-liquid fuel strategies, with emphasis being placed on thermochemical processes[15–17] and depolymerization of biomass into intermediates followed by hydrodeoxygenation (HDO).[14,18,19] Both strategies have their own merits. Still, thermochemical approaches have been implemented with limited success due to the significant investment required to implement these units at large scale. At the same time, lignocellulosic biomass deconstruction followed by HDO strategies remains at earlier stages of development. In addition, this new and renewable industry will compete with the well-established oil industry. In light of these observations, the integration of existing technological and logistics platforms into oil refineries with large-scale biomass conversion units appears to be crucial.
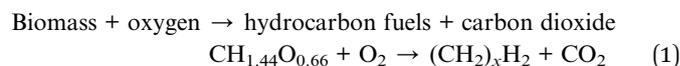
One of the main areas of interest is the production of sustainable biofuels from lignocellulosic biomass and its derivatives using zeolites as catalysts. This would enable a rapid transition from petroleum to low-carbon index drop-in biofuels. However, effective and robust technologies for the commercial-scale production of biofuels using zeolites have yet to be developed. This review summarizes the latest developments in this field, focusing on the catalytic transformation of lignocellulosic carbohydrates and lignin and their derivatives into biofuels (alkanes, aromatics and oxygenated biofuels) using zeolites as catalysts. Given the number of comprehensive reviews in the literature on biomass pyrolysis with zeolites,[20–22] this topic is beyond the scope of this review.

1.1. Lignocellulosic biomass

Today, most biofuels are produced from vegetable oils (e.g., soybean), starches (e.g., corn), and sugar (sugarcane).[23] However, the supply of these substrates is not large enough to meet the demand for biofuels, and it competes with food production. Lignocellulosic feedstocks (e.g. wood, straw and grasses) are highly abundant and have been used as a source of energy. About 100 billion tons of biomass containing about 50% carbon (mass basis) is produced annually and can be converted into biofuels.[24] Much more lignocellulosic biomass can be sustainably produced, if needed.[23,25]

Biomass can be used as a feedstock to produce liquid fuels, as shown in eqn (1). Biomass can be used as a carbon source to produce a hydrocarbon product, a carbon source to remove oxygenated groups from biomass as CO_2, and an energy source for transformation processes.[23]

$$\text{Biomass} + \text{oxygen} \rightarrow \text{hydrocarbon fuels} + \text{carbon dioxide}$$
$$CH_{1.44}O_{0.66} + O_2 \rightarrow (CH_2)_xH_2 + CO_2 \qquad (1)$$

This can be achieved by converting lignocellulosic substrates into platform chemicals. This involves partial deoxygenation, catalytic upgrading to the target molecules through C–C coupling reactions and removal of remaining oxygen groups.[26] Although lignocellulosic biomass is the most inexpensive and abundant form of biomass, it is challenging to convert it into fuels due to its solid form and low energy density.[27] Also, depending on the biomass source, impurities such as metal contaminants may be present, which affect catalyst performance (especially solid catalysts) and downstream processing.[28,29] Lignocellulosic biomass is also a rather complex substrate due to the intrinsic heterogeneity of its components, which makes its conversion challenging.[28] It is composed of cellulose (40–50%), hemicelluloses (20–40%), and lignin (18–35%). Proteins, waxes, and phenolic compounds constitute up to 10% of the biomass dry weight.[30] While cellulose is a homopolysaccharide composed of glucose units linked by β-1,4-glycosidic bonds, hemicelluloses can be described as both branched and amorphous heteropolymers composed of D-xylose, D-mannose and D-glucose.[31] Lignin is also a heterogeneous polymer, but it is composed of p-hydroxyphenyl, guaiacyl, and syringyl as the main phenylpropanoid units.[31] These units are linked through C–O (e.g. β–O–4, 4–O–5, and α–O–4) and C–C (e.g. β–5, β–β, β–1, and 5–5) bonds, forming a highly complex polymer.[32] The content of these bonds varies with the type of lignocellulosic feedstock. Generally, ether bonds account for over 50% of the lignin bonds. Softwoods and hardwoods are composed of 43% and 65% of β–O–4 linkages, respectively.[32,33] Due to lignocellulosic biomass complexity, the conversion of lignocellulosic biomass into fuels often requires a cascade of reactions. Each reaction step may require different operational conditions, and several of the intermediate compounds produced are unstable. In this case, the use of catalysts with multiple active sites for the direct conversion of biomass can be advantageous, as it does not require catalyst separation after each reaction step.[34]

1.2. Zeolites as catalysts

The transformation of lignocellulosic feedstocks and their precursor molecules into biofuels involves many acid-catalyzed

reactions (e.g. hydrolysis, alkylation and isomerization).[34] Homogeneous catalysts, such as mineral acids, are more active than solid catalysts due to their enhanced mass transfer.[35] However, homogeneous catalysts often face challenges, such as product separation and corrosion. Also, they require downstream processing,[36] which limits their industrial applications.[37] Acidic zeolites are a promising alternative to homogeneous catalysts because of their thermal stability, market availability, and recyclability.[38,39] Among the primary applications of synthetic zeolites (e.g., catalysis, detergents, and adsorbents), catalysis represents about 20% of the volume and contributes about 50% of the total revenue.[40] As of 2010, the worldwide production of synthetic zeolites reached about 4 million tons per year, valued at around 3 billion US$.[40] The International Zeolite Association (IZA) has reported over 250 different zeolite topologies.[41] Zeolites are crystalline and microporous aluminosilicates with properties that can be tailored to specific applications.[42] Acidic zeolites have Brønsted and Lewis acidity (attributed to framework and/or extra framework Al atoms) and well-defined pores that are made of SiO_2 and AlO_4 tetrahedra.[34,43] Their crystals are highly microporous (from about 0.4 nm to up to tens of nanometers in special zeolites),[44] which contain the catalytic sites and the properties responsible for shape selectivity. Their highly tunable textural and acidic properties enable high surface areas, molecular diffusion control, and easy regeneration at elevated temperatures.[34] The density and strength of the acid sites can be fine-tuned by adjusting framework composition (i.e., Si/Al ratio) and by incorporating redox-active transition metals (e.g., Ni, Co and Cu) into the framework (i.e., adjusting Lewis acid density).[45] Highly tunable acidity is critical to induce C–O bond cleavage, while preserving or forming C–C bonds. This acidic property of zeolites enables the transformation of raw lignocellulosic biomass and its derived molecules into desirable fuel precursors.[11,46] For example, weak acid sites facilitate ether bond rearrangement and lignin side-chain cleavage, while medium and strong acid sites contribute to deoxygenation reactions.[47] Also, the literature has shown that acid density plays a key role in catalyst stability. While coke formation can occur on both weak and strong acid sites of a zeolite, decreased strong acid sites have been identified as a significant contributor to coke formation/deposition reduction.[48] However, as micropores contain the active sites, the diffusion of bulky lignocellulosic biomass molecules in and out of the pores is mass-transfer limited.[49,50] In this case, catalytic activity occurs mainly at the active sites located on the external surface of the zeolite.[51] This leads to underutilization of the active sites, low product yields, and low product selectivity, as well as potential catalyst deactivation due to the formation and/or deposition of coke.[52,53] In addition to the moisture present in raw lignocellulosic biomass (5–30%),[54,55] many reactions involving lignocellulosic biomass-derived molecules generate water as a by-product.[56] The production of water can cause crystallinity decrease and irreversible deactivation of the zeolite in an elevated temperature aqueous environment, leading to low catalyst activity, recyclability, and lifetime.[57–59]

To address these challenges, several strategies ranging from pre-processing of biomass feedstocks to inducing mesoporous structures within the acidic zeolites have been developed. Hierarchical zeolites, which have additional mesopores (2–50 nm) or macropores (>50 nm), have been shown to address these challenges by providing easier access to the active sites. Hierarchical zeolites have an additional network of larger pores that overlays and interconnects with the micropores.[46] These pore networks improve diffusivity and can develop either in the zeolite crystals as intracrystalline porosity or between the crystals as intercrystalline porosity.[53,60] Relative to ordered mesoporous materials, such as MCM-41, hexagonal mesoporous silica (HMS) and SBA, hierarchical zeolites have a crystalline structure, higher thermal and hydrothermal stability, and generally higher acidity.[61] Such properties have resulted in enhanced zeolite performance in various reactions, including hydrolysis of cellulose and hemicellulose, lignocellulose pyrolysis, HDO of lignin, and selected condensation reactions.[62–64] For example, in the HDO of lignin over hierarchical zeolites, bulky oxygen-containing compounds are cleaved into smaller molecules by acid sites on the mesoporous surface, allowing their access to microporous channels for further transformation. Also, hierarchical zeolites provide additional entry points for macromolecular oxygenated compounds and enhance intracrystalline transport, which increases reaction rates by decreasing coke deposition.[65,66] The introduction of mesoporosity into a zeolite structure not only reduces the steric and/or diffusional limitations of bulky biomass molecules but also provides an opportunity to fine-tune the acidity of the catalyst.[67,68] While hierarchical zeolites offer several highly desirable properties, they also tend to show less "zeolitic behavior" in terms of acidity, hydrophobic/hydrophilic balance, confinement effects, shape selectivity, and hydrothermal stability compared to microporous zeolites.[65]

Hierarchical zeolites have been synthesized through a variety of synthesis methods, including "bottom-up" (e.g., soft templating, hard templating, and template-free) that involves the preparation of nanostructures of larger size units, and "top-down" (e.g., dealumination, desilication, and dissolution–recrystallization) that involves the assembly of several small structural ones, and nanozeolite assembly (Fig. 1).[46,69]

Details on the synthesis methods of hierarchical zeolites have been extensively reviewed and summarized in various review articles in the last few years.[46,60,70,71] It should be pointed out that the introduction of mesoporosity into microporous zeolites is not always easily reproducible, leading to different catalytic performances, because both nucleation and crystallization are complex processes.[67] Hierarchical zeolites synthesized through mesostructuring, also known as surfactant templating (where CTAB and a base, NaOH or NH_4OH, were used concurrently), showes uniform intracrystalline mesopores with a shape resembling that of a regular hexagonal unit of MCM-41.[72] These zeolites usually show enhanced product selectivity, due to uniform mesopores and lower coke deposition. Note that mesostructuring had only been successfully synthesized in Y, β, modernite, LTL, and omega zeolites, due to their low framework density. In contrast, no mesostructured
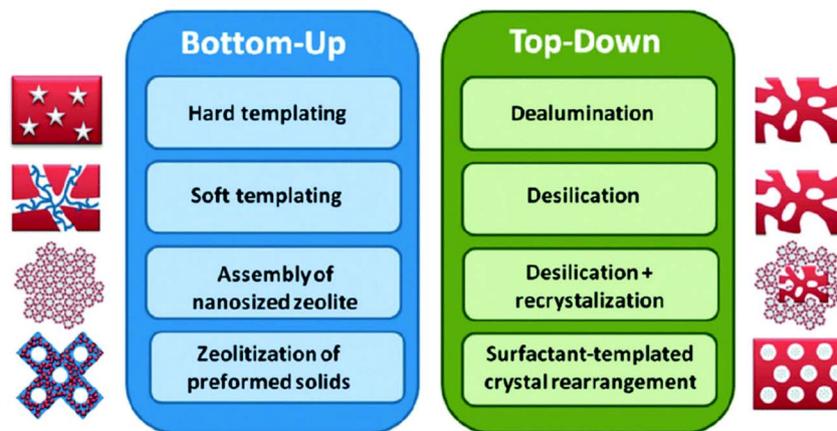
Fig. 1 Methods used to prepare hierarchical zeolites. Reprinted from ref. 46 with permission from [John Wiley & Sons], Copyright [2014].

ZSM-5 zeolite has been synthesized.[72] While excellent reviews on the use of zeolites for biomass conversion, focusing on hierarchical zeolite design[73] and catalytic biomass reactions, can be found in literature,[26,74] most do not include the latest advancements in the field. This review aims to provide an up-to-date perspective on the direct production of biofuels, including alkanes, aromatics and oxygenated biofuels, from raw lignocellulosic biomass and their derived components over both microporous and hierarchical zeolite-based catalytic systems. Furthermore, we explore the main challenges associated with the use of zeolites as acidic catalysts for lignocellulosic biomass processing and discuss possible approaches to overcoming such challenges.

2. Raw lignocellulosic biomass as a substrate

A direct route to convert lignocellulose to liquid alkanes and its integration within refineries would enable a fast commercial process implementation, as the renewable products can be processed using the existing refinery assets with a relatively small investment.[75] However, research on one-pot processes for catalytic transformation of biomass to hydrocarbon fuels using zeolites is scarce in the literature. The selective removal of oxygen-containing groups from biomass polymers without breaking C–C bonds remains a significant challenge. Also, biomass materials with distinct macromolecular compositions and morphological structures should be used as substrates to evaluate the robustness of the process in converting a wide range of biomass types, notably hardwoods and softwoods. Thus, research going forward should address key challenges specific to herbaceous biomasses, including monocots and dicots, as well as solid loadings required for industrial processes. Xia *et al.* were the first group to report the conversion of birch wood to liquid hydrocarbons with high selectivity towards pentane (4.9 wt% yield) using 5 wt% Pt/H-ZSM-5 at 190 °C and 5 MPa H_2 for a 20 h residence time. Under these conditions, the total hydrocarbon yield was 8 wt%.[76] Siakpebru *et al.* reported an efficient one-pot process to convert poplar

biomass into liquid hydrocarbons in cyclohexane over 10 wt% Ni/H–β.[75] An alkane liquid and aromatic yield (carbon-based) of ~16 wt% and high selectivity toward C_7–C_{15} cycloalkanes (~8%) from poplar were obtained at 270 °C, 6 h, and an initial H_2 pressure of 3 MPa. 10 wt% Ni/H–β resulted in higher carbon liquid yields than other catalyst supports (H-ZSM-5 and H-USY) with 10% Ni loading. This improvement was explained by the Brønsted acidity of H–β and strong metal–support interactions between Ni particles and the H–β support, which effectively catalyze both hydrogenation and hydrogenolysis pathways. Also, 10% Ni/H–β showed good recyclability over two recycling runs, with an ~18% decrease in liquid yields after the first recycling cycle. A significant reduction in Brønsted and strong acid sites was observed in the regenerated catalyst, which was attributed to the production of water as a by-product during HDO. The formation of water has a negative impact on zeolite catalysts, namely during the calcination and regeneration steps. Hydrothermal steaming causes the loss of framework aluminum from H–β zeolites, which results in lower Brønsted acidity and, consequently, lower catalytic performance. To address this challenge, different strategies, such as coating acidic zeolites with organic silanes to protect framework aluminum and the use of rare earth oxides (*e.g.*, La_2O_3 and CeO_2) to stabilize the framework aluminum in H–Y zeolites, have been explored.[58,77] While these approaches have shown some success, they often lead to reduced BET surface area and pore volume, which can negatively impact catalytic performance.

For higher-chain hydrocarbon fuels, such as SAFs and renewable diesel, no reports have been found in the literature on the direct HDO of lignocellulosic biomass using zeolites. Some zeolites can be strongly acidic, but they lack the textural properties needed to enhance the production of bulky molecules (C_8–C_{20}). Acidic hierarchical zeolites with increased mesoporosity and pore size are a promising alternative. For instance, Siakpebru *et al.* reported a hydroxyalkylation-alkylation (HAA) reaction between biomass-derived molecules, such as 2-methylfuran (2 MF) and furfural, which resulted in a 72 mol% yield of a C_{15} jet fuel precursor using a hierarchical

H–Y zeolite.[78] The superior performance of the hierarchical H–Y relative to parental H–Y was attributed to its strong Brønsted acidity and large external surface area.

3. Conversion of lignocellulosic carbohydrates

3.1. Cellulose

Cellulose is a highly available, linear homopolysaccharide composed of glucose monomers. Its repeating structural unit is either cellobiose or 4-O-β-ᴅ-glucanopyranosyl-ᴅ-glucopyranose.[79] It is considered an ideal substrate for the selective production of C_6 alkanes (*i.e.*, light naphtha), as C–C bond formation or cleavage is not required.[80] The main challenges associated with the conversion of cellulose into C_6 alkanes are the selective cleavage of C–O linkages and removal of surplus oxygen, while preserving C–C linkages during deoxygenation. Other challenges include low solubility in conventional fluids and high chemical resistance.[81] The overall process of converting cellulose into alkanes is rather complex, involving a series of sequential reactions (*e.g.* hydrolysis, hydrogenolysis, hydrogenation, dehydration, and HDO).[82] As such, severe operating conditions (*i.e.* high temperature, long reaction times, and catalyst acidity) are required, but they can also lead to undesirable side reactions.[80] To effectively manage these sequential steps and overcome the inherent drawbacks associated with cellulose conversion, zeolites loaded with a metallic component as bifunctional catalysts have been studied. Table 1 provides a comprehensive overview of the diverse reaction conditions and zeolite-based catalysts used to convert cellulose and its derivatives into C_6 alkanes. Although the HDO of cellulose-derived water-soluble sugars and sugar alcohols into liquid fuels has been widely reported (see Section 3.2), the direct production of alkanes from cellulose is highly desirable as it would reduce the number of processing steps and, therefore, have higher economic efficiency.[83] For example, the direct conversion of cellulose to *n*-hexane has been reported by Liu *et al.*, who found that Ir–ReO$_x$/SiO$_2$ (Re/Ir = 2) and H-ZSM-5 (as a co-catalyst) resulted in an *n*-hexane yield of 83% and 78% from ball-milled cellulose and microcrystalline cellulose, respectively.[84] Reports found in the literature show that Ir–ReO$_x$/SiO$_2$ can effectively promote the hydrogenolysis of C–O bonds.[85] The authors suggested that (1) the hydrolysis of cellulose into glucose through water-soluble oligosaccharides is catalyzed by H-ZSM-5 and is identified as the rate-determining step, (2) Ir–ReO$_x$/SiO$_2$ catalyzed the hydrogenation of glucose to sorbitol, and (3) hydrogenolysis of sorbitol into *n*-hexane was catalyzed by both Ir–ReO$_x$/SiO$_2$ and HZSM-5 (Fig. 2).[84]

Although the reported *n*-hexane yields are encouraging, high temperatures (210 °C), H_2 pressures (6 MPa of initial pressure), and long reaction times (24 h) were required to convert pristine, microcrystalline cellulose into *n*-hexane. However, when cellulose was pretreated *via* ball-milling (to reduce the crystalline content, thus increasing the reactivity of cellulose to chemical treatment), shorter reaction times were used. Although long reaction times were needed, the catalytic system demonstrated

potential for recycling. The yield of *n*-hexane only decreased from 83 to 71% in the first recycling run. However, by the third recycling, aggregation of Ir during regeneration was observed, which resulted in a decreased *n*-hexane yield to 66%.

Also, the potential of Ir–VO$_x$/SiO$_2$ combined with HZSM-5 to catalyze the conversion of cellulose into C_5/C_6 alkanes at relatively low temperatures of 210 °C was investigated by Jin *et al.*[86] It was found that the V/Ir molar ratio critically impacted the C_5/C_6 alkane yield. Increasing the V/Ir molar ratio from 0 to 0.13 significantly increased the yield of C_5/C_6 alkanes from 46.4 to 78.7% because vanadium acts as a good metal promoter for Ir. However, further increases in the V/Ir ratio led to a significant decrease in yield. This reduction was explained by the partial reduction of Ir caused by an excess of vanadium, which negatively impacted the hydrogenation performance.[87] In contrast, excess vanadium increases the acid sites, promoting isomerization and cyclic ether formation.[86] This catalytic system (Ir–VO$_x$/SiO$_2$ combined with HZSM-5) showed acceptable reusability. The C_5/C_6 yield decreased from 78.7% (fresh run) to 43.5% (5th recycling run), and the accumulation of Ir was considered to be the main reason for the observed decrease in yield.[86] The same group reported that Mo-promoted Ir/SiO$_2$ (0.5 Mo/Ir molar ratio) combined with H-ZSM-5 achieved ~92% C_5/C_6 alkane yield from microcrystalline cellulose at 210 °C for 12 h and in a biphasic system (*n*-dodecane and H_2O).[82] The superior yield was attributed to the enhanced hydrogenation performance of the Ir–MoO$_x$/SiO$_2$ through hydrogen spillover from Ir particles to MoO$_x$ species. The addition of H-ZSM-5 further enhanced the Ir–MoO$_x$/SiO$_2$ hydrogenolysis activity, with sorbitol being the major intermediate product.[82]

Kato and Sekine reported that the direct catalytic transformation of cellulose resulted in high total C_3 and C_4 selectivity (46.8 %C) when the H–β zeolite + Pt/γ-Al$_2$O$_3$ catalytic system was used at 170 °C.[88] While the authors tested different catalysts, such as γ-Al$_2$O$_3$, H–β, H–β + γ-Al$_2$O$_3$, H–β + Pd/γ-Al$_2$O$_3$, H–β + Co/γ-Al$_2$O$_3$, H–β + Cu/γ-Al$_2$O$_3$, H–β + Ni/γ-Al$_2$O$_3$, and H–β + Fe/γ-Al$_2$O$_3$, only the H–β + Pt/γ-Al$_2$O$_3$ catalyst was found to be effective in converting cellulose-derived compounds into C_3 and C_4 hydrocarbons due to the synergistic activities of Pt and H–β, including decarbonization, dehydrogenation, and cracking/hydrogenolysis. In addition, zeolites with large pores and a low Si/Al ratio have been reported as effective catalysts for cellulose hydrolysis.[88] Such properties facilitate the diffusion of cellulose-derived products, such as glucose, which enhances their access to zeolite acid sites.

Murata *et al.* investigated the conversion of cellulose into C_2–C_9 paraffins over H-ZSM-5 (SiO$_2$/Al$_2$O$_3$ = 23) and H-USY (SiO$_2$/Al$_2$O$_3$ = 6.3) loaded with 1 wt% Pt at 400 °C and 6.5 MPa for 12 h.[89] The authors found that both 1 wt% Pt/H-USY and 1 wt% Pt/H-ZSM-5 resulted in similar C_2–C_9 selectivity, while 1 wt% Pt/H-ZSM-5 resulted in higher selectivity toward CH$_4$. However, the authors did not explain the reason for higher CH$_4$ selectivity with 1 wt% Pt/H-ZSM-5. Also, 1 wt% Pt/H-ZSM-5 led to a total alkane selectivity of ~78%. To reduce the amount of CO$_x$ and CH$_4$, cellulose was pretreated with alcohols (*e.g.* 1-propanol, 1-butanol, 1-pentanol, 1-hexanol, *etc.*) before hydrocracking.[89] When cellulose was pretreated with 1-hexanol at 350 °C

Table 1 Overview of the zeolite-based processes used to convert cellulose and its derivatives into biofuels

Feedstock	Reaction conditions	Catalytic systems	Solvent	Reactor type	Product yield and selectivity	Ref.
Microcrystalline cellulose	250 °C, 24 h, 6 MPa initial H_2 pressure	Ir–ReO$_x$/SiO$_2$ combined with HZSM-5	n-dodecane/water	Batch	Cellulose conversion: 99%; n-hexane yield: 78%	84
Microcrystalline cellulose	210 °C, 12 h, 2–8 MPa initial H_2 pressure	Ir–MoO$_x$/SiO$_2$ combined with HZSM-5	n-dodecane/water	Batch	Cellulose conversion: >99.9%; C$_5$/C$_6$ alkane yield: 91.7%	82
Microcrystalline cellulose	210 °C, 24 h, 6 MPa initial H_2 pressure	Ir–VO$_x$/SiO$_2$ combined with HZSM-5	n-dodecane/water	Batch	Cellulose conversion: ~100%; 85.1% C$_5$/C$_6$ alkanes yield	86
Ball-milled cellulose (ball-milling time of 2 h)	240 °C, 12 h, 6 MPa initial H_2 pressure	Ir–ReO$_x$/SiO$_2$ combined with HZSM-5	n-dodecane/water	Batch	Cellulose conversion: 93%; n-hexane: 83%	84
Ball-milled cellulose	170 °C, 3 h, Ar atmosphere	0.9 wt% Pt/USY	Water	Batch	Cellulose conversion: >19.4%; total hydrocarbon yield: 1.5 %C, C$_3$–C$_5$ olefin selectivity: 0.9 %C^a	90
Ball-milled cellulose	170 °C, 72 h, Ar atmosphere	1 wt% Pt/NH$_4$–USY	Water	Batch	C$_3$ + C$_4$ hydrocarbon yield: 14.5 %C	91
Pretreated cellulose (with 1-hexanol, 350 °C, 2 h)	400 °C, 12 h, 6.5 MPa N$_2$/N$_2$ (85 : 15 vol.%)	1 wt% Pt/ZSM-5	Water	Batch	100% yield into alkanes and CO$_x$; carbon selectivity: 3.1% (CH$_4$), 42.1% (C$_2$–C$_4$), 47.0% (C$_5$–C$_9$), 4.4% (C$_{10}$–C$_{20}$) and 0.43% (C$_{21+}$)	89
Cellulose	170 °C, 3 h, 6 MPa H_2	1 wt% Pt/H–β	Water	Batch	Cellulose consumption: 448.2 C-μmol; C$_3$ + C$_4$ hydrocarbons amount − 169.59 C-μmol	88
Cellulose	400 °C, 12 h, 6.5 MPa N$_2$/N$_2$ (85 : 15 vol.%)	1 wt% Pt/USY	Water	Batch	97.2% yield into alkanes and CO$_x$; carbon selectivity: 12% (CH$_4$), 20.6% (C$_2$–C$_4$), 17.8% (C$_5$–C$_9$), 14.5% (C$_{10}$–C$_{20}$) and 3.96% (C$_{21+}$)	89
Cellulose	400 °C, 12 h, 6.5 MPa N$_2$/N$_2$ (85 : 15 vol.%)	1 wt% Pt/ZSM-5	Water	Batch	69.7% yield into alkanes and CO$_x$; carbon selectivity: 28.7% (CH$_4$), 19.0% (C$_2$–C$_4$), 18.6% (C$_5$–C$_9$), 21.0% (C$_{10}$–C$_{20}$) and 1.21% (C$_{21+}$)	89
Cellobiose	140 °C, 108 h, 8 MPa H_2	Ir–ReO$_x$/SiO$_2$ combined with HZSM-5	n-dodecane/water	Batch	Cellobiose conversion: >99.9 %C; n-hexane yield: 94.8 %C	92
Cellobiose	170 °C, 3 h, Ar atmosphere	0.9 wt% Pt/USY	Water	Batch	Cellobiose conversion: >94.2%; total hydrocarbon yield: 2.2 %C, C$_3$–C$_5$ olefin selectivity: 69.3 %C^a	90
Glucose	140 °C, 84 h, 8 MPa H_2	Ir–ReO$_x$/SiO$_2$ combined with HZSM-5	n-dodecane/water	Batch	Glucose conversion: >99.9 %C; n-hexane yield: 94.4 %C	92
Glucose	170 °C, 3 h, Ar atmosphere	0.9 wt% Pt/USY	Water	Batch	Glucose conversion: >82.4%; total hydrocarbon yield: 2.0 %C, C$_3$–C$_5$ olefin selectivity: 79.5 %C^a	90
Glucose	200 °C, 5 h	HY-PrSO$_3$H	Ethanol	Batch	EL yield: 57.6%	101
Glucose	160 °C, 2h	HPW/H-ZSM-5	Ethanol	Batch	EL yield: 19.1%	102
Glucose	200 °C, 10 min	USY	Ethanol/THF	Batch	Glucose conversion: 98%; EMF yield: 42%; EL yield: 5%	103
Glucose	200 °C, 10 min	USY	Ethanol	Batch	Glucose conversion: >97%; EM yield: 33%, EL yield: 15%	103
Glucose	180 °C, 2 h	USY	Ethanol	Batch	EL yield: 48%	104
Glucose	180 °C, 2 h	H$_2$SO$_4$/USY	Ethanol	Batch	EL yield: 51.5%	105
Sorbitol	240 °C, 1 h, 4 MPa H_2	10% Ni/HZSM-5	Water	Batch		95

Table 1 (Contd.)

Feedstock	Reaction conditions	Catalytic systems	Solvent	Reactor type	Product yield and selectivity	Ref.
Fructose	170 °C, 3 h, Ar atmosphere	0.9 wt% Pt/USY	Water	Batch	i-C_6H_{14} selectivity: 45.4%; total i-C_6H_{14} and i-C_5H_{12} yield: 32.3%	90
Fructose	200 °C, 5 h	HY-PrSO$_3$H	Ethanol	Batch	Fructose conversion: >95.8%; total hydrocarbon yield: 1.2 %C, C_3–C_5 olefin selectivity: 65 %C[a]	101
Fructose	160 °C, 2 h	HPW/H-ZSM-5	Ethanol	Batch	EL yield: 63.7%	102
Fructose	140 °C, 24 h	H–Y	Ethanol	Batch	EL yield: 43.1%	106
Sorbitol	240 °C, 1 h, 4 MPa H$_2$	2% Ni/HZSM-5 modified with 40 wt% MCM-41	Water	Batch	Fructose conversion: 93%; EL yield: 8%	98
Sorbitol	260–350 °C, 4 MPa H$_2$, 150 mL min^{-1} H$_2$ flow	Mesoporous Ni/SG-Ni/H-ZSM-5	—	Fixed-bed	Sorbitol conversion: 67.1%; liquid alkane selectivity: 98.7%	100
Sorbitol	320 °C, 4 MPa H$_2$, 150 mL min^{-1} H$_2$ flow	10% Ni-HZSM-5 mixed with SBA-15	Water	Fixed-bed	Carbon yield of long-chain alkanes (C_5–C_{12}): Up to 46.94%	99
Sorbitol	425 °C, 1.0 h^{-1} weight hourly space velocity	ZSM-5 -WOS (28)	—	Fixed-bed	Oil yield: 40.4 wt%; oil content: 80% in aromatics and cyclic hydrocarbons	107
HMF	150 °C, 12 h	Hierarchical ZSM-5	Ethanol/n-hexane	Batch	Sorbitol conversion: 92%; pentane selectivity: 48%	108
Levulinic acid	78 °C, 5 h	H–β	Ethanol	Batch	HMF conversion: 94.2%; EL selectivity: >90.8%	109
Levulinic acid	120 °C, 7 h	Desilicated H-ZSM-5	Ethanol	Batch	LA conversion: 40%; EL selectivity: 98%	110
Levulinic acid	120 °C, 7 h	Dodecatungstophosphoric acid/desilicated H-ZSM-5	Ethanol	Batch	LA conversion: 95%; EL selectivity: 100%	111
					LA conversion: 94%; EL selectivity: 100%	

[a] C_3 – C_5 olefin selectivity = $\frac{C_3 - C_5\ \text{yield}}{C_3 - C_5\ \text{olefin yield} - C_3 - C_5\ \text{paraffin yield}} \times 100$
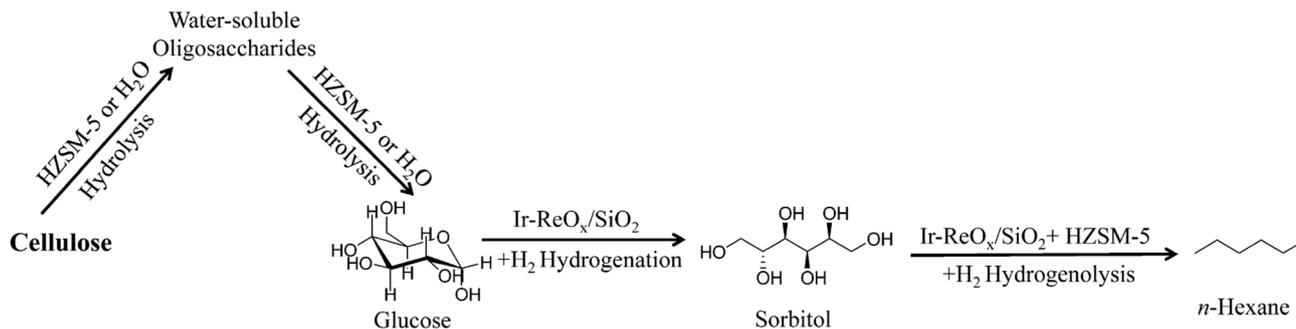
Fig. 2 Illustration of the reaction pathways for cellulose conversion into *n*-hexane using H-ZSM-5 and Ir–ReO$_x$/SiO$_2$. Reprinted from ref. 84 with permission from [American Chemical Society], Copyright [2015].

followed by hydrocracking over 1 wt% Pt/H-ZSM-5 (SiO$_2$/Al$_2$O$_3$ = 23), a CH$_4$/CO$_x$ yield of only 6% was reported. It was hypothesized that the cellulose pretreatment reduces the cellulose molecular weight, forming oxygenated intermediates, which are then converted into alkanes through hydrocracking and condensation reactions.[89]

Ogo *et al.* investigated a Pt/USY zeolite catalyst for converting cellulose into C$_3$ and C$_4$ hydrocarbons.[90] The authors reported that the acid sites of H-USY were mainly responsible for the solubilization of cellulose into sugars, while Pt sites promoted their cracking into hydrocarbons. In addition, olefin selectivity was highly impacted by the oxidation state of the supported Pt, which was influenced by the catalyst pretreatment. Higher olefin selectivity was reported for air-oxidized Pt/H-USY than that of the H$_2$-reduced catalyst.[90] The same group also reported a Pt/NH$_4$-USY catalyst, resulting in a C$_3$ and C$_4$ hydrocarbon yield of 14.5 %C from cellulose at 170 °C for a reaction time of 72 h.[91] Both Pt/H-USY and Pt/NH$_4$-USY catalysts showed high hydrothermal stability at 170 °C, and no metal leaching was reported.[90,91]

3.2. Cellulose intermediates

In this section, we reviewed the direct production of C$_5$ and C$_6$ alkanes *via* HDO of cellulose-derived compounds, including monosaccharides (glucose and fructose), disaccharides (cellobiose), and polyols (sorbitol). Such intermediates can also be referred to as platform chemicals. Monosaccharides and polyols have a carbon-to-oxygen ratio of 1 : 1, which allows them to be converted into hydrocarbon fuels through a series of C–C and C–O cleavage reactions. These reactions result in a range of mono-functional organic compounds (*e.g.* ketones, alcohols, carboxylic acids, and furfurals) that further undergo C–C coupling (*e.g.* aldol condensation, ketonization, and oligomerization) and deoxygenation reactions.[26]

Chen *et al.* investigated the conversion of cellobiose and glucose into *n*-hexane using Ir–ReO$_x$/SiO$_2$ combined with H-ZSM-5.[92] The reason behind the use of H-ZSM-5 as a co-catalyst is that it enhances the dehydration of secondary alcohols, which promotes their conversion to alkanes through hydrogenolysis. This dehydration–hydrogenation pathway is critical for the conversion of internal mono-ols to alkanes and the suppression

of undesirable C–C cracking reactions. However, the authors found that extremely long reaction times (*i.e.*, 108 h) are needed to obtain an *n*-hexane yield of 95 %C from cellobiose at 140 °C and a H$_2$ pressure of 8 MPa. At a reaction time of 24 h, only 19.1 %C was obtained. Even though the results obtained at long reaction times are encouraging, much shorter reaction times are needed to further develop this technology for commercial applications. Interestingly, even when glucose was used as a model feedstock, long reaction times were still needed (84 h) to achieve an *n*-hexane yield of 94.4 %C. Although long reaction times are required, this catalytic system resulted in high yields of *n*-hexane (over 90 %C) in the first three recycling runs. By the 4th recycling run, the amount of *n*-hexane formed was lower compared to a fresh catalyst run under similar conditions. Ogo *et al.* also tested Pt/H-USY to convert glucose into hydrocarbons at 170 °C for 3 h.[90] They reported a glucose conversion of 82.4% and a high selectivity of 79.5% toward C$_4$ olefins. The number of reports on the conversion of glucose into alkanes is scarce because most studies use glucose, cellobiose, and fructose as substrates mainly to investigate reaction mechanisms rather than to optimize alkane yields.

The conversion of sorbitol involves aqueous-phase reforming over a metal catalyst, such as Ni and Pt, during which hydrogen and CO$_2$ are generated, and dehydration reactions over solid acid catalysts, such as zeolites, which lead to the formation of oxygenated intermediates.[93] The hydrogen produced hydrogenates these intermediates over the metal sites. Through consecutive cycles of dehydration/hydrogenation reactions, oxygen is removed, leading to the production of alkanes.[93] The proposed reaction pathways were reported by Huber *et al.* and are shown in Fig. 3.[94]

Zhang *et al.* studied the production of isoparaffins from sorbitol over Ni/H-ZSM-5 catalysts.[95] Zeolite H-ZSM-5 is known to induce isomerization of paraffins, which improves the octane number of such paraffins.[96,97] The authors found that the catalyst's calcination temperature is critical to increase *i*-C$_6$H$_{14}$ and *i*-C$_5$H$_{12}$ selectivity. For example, when the calcination temperature increased from 400 °C to 500 °C, the selectivity of *i*-C$_6$H$_{14}$ increased from 20.3 to 45.4%.[95] However, further increases in calcination temperatures resulted in a significant drop in *i*-C$_6$H$_{14}$ selectivity to 25%. This suggests that the catalyst calcined at 500 °C is critical to provide the highest selectivity toward
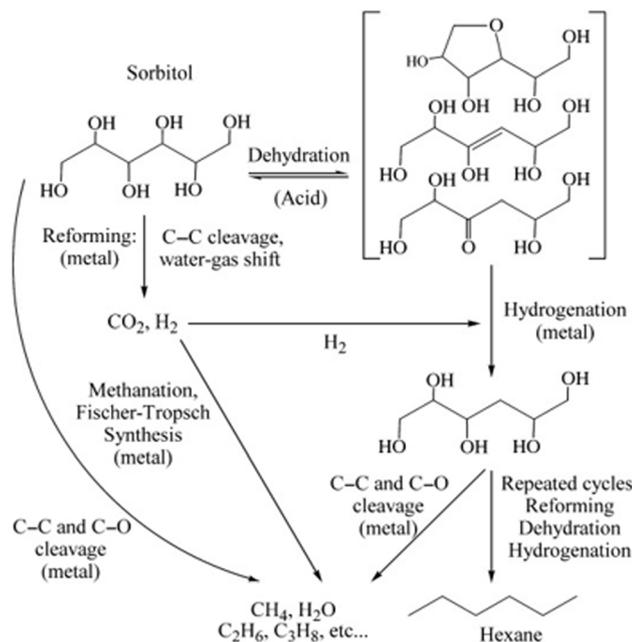
Fig. 3 Proposed reaction pathways for the production of alkanes from sorbitol. Reprinted from ref. 94 with permission from [John Wiley & Sons], Copyright [2004].

isoparaffins, due to an optimal balance between acidity, structural properties, and Ni species reducibility. It was hypothesized that high temperatures are associated with the sintering of Ni and dealumination of zeolite, leading to lower acidity.[95] Also, Zhang et al. studied the conversion of sorbitol into C_5 and C_6 alkanes over Ni/HZSM-5 modified with MCM-41 at 240 °C and a H_2 pressure of 4 MPa.[98] While Ni/HZSM-5 was mainly responsible for the C–C cleavage in sorbitol into C_1–C_4 alkanes due to its strong Brønsted acid sites, MCM-41 catalyzed the C–O bond cleavage into heavier alkanes due to its weak Lewis acid sites. In addition to their acidic nature, MCM-41 offers larger pore sizes and high surface areas, which enhance mass transfer of bulky intermediates and reduce diffusion limitations. A total alkane yield of 98.7% was found when 2% Ni/HZSM-5 modified with 40 wt% MCM-41 was used. Also, the same group reported that the addition of MCM-41 reduced carbon deposition on the surface of Ni/H-ZSM-5. However, further studies are needed to evaluate the hydrothermal stability and recyclability potential of the proposed catalytic system.

Weng et al. also studied the production of aromatics and cyclic hydrocarbons from the conversion of sorbitol catalyzed by

Ni-HZSM-5 mechanically mixed with SBA-15.[99] This catalytic system has a bimodal pore structure, combining the micropores of H-ZSM-5 with the mesopores of SBA-15, which enhances accessibility for larger molecules and their transport between active sites. This catalytic system allowed large sorbitol molecules to be initially hydrodeoxygenated by Ni-SBA-15 into smaller oxygen-containing compounds, which then enter the H-ZSM-5 pores for further reaction. A maximum oil yield of 40.4 wt% was obtained at 320 °C and a H_2 pressure of 4 MPa, with aromatics and cyclic hydrocarbons making up 80% of the final product. The authors pointed out that the temperature used (i.e., 320 °C) was significantly lower than the typical temperatures used in conventional aromatization processes (350–500 °C). The same group also reported the one-pot aqueous catalytic conversion of sorbitol into gasoline using a physically mixed Ni/HZSM-5 and Ni/silica-gel (mesoporous SG) catalytic system in a fixed-bed reactor.[100] Adding mesoporous SG into Ni/H-ZSM-5 enhanced the carbon yield of C_5–C_{12} alkanes up to ~47% at 300 °C and 4 MPa H_2 pressure. The addition of mesoporous materials, such as silica gel, helped modulate the acidity of H-ZSM-5, shifting the product selectivity from C_1–C_4 alkanes (resulting from C–C cleavage on strong Brønsted acid sites) to long carbon chain (C_5–C_6 or C_5–C_{12}) alkanes (from C–O cleavage on weaker Lewis acid sites). In addition, the synergistic effects of physically mixing catalysts, such as mesoporous SG with Ni/H-ZSM-5, are the integration of HDO, ketonization, and aldol–condensation reactions, which enhances the formation of additional C–C bonds and the production of long-chain alkanes. These processes typically occur at lower temperatures (280–320 °C) than those used in methanol-to-gasoline reactions (350–500 °C), improving energy efficiency and reducing coke formation. Although promising results were obtained to produce long-carbon-chain hydrocarbons from sorbitol using Ni/HZSM-5 and Ni/silica-gel (mesoporous SG), further studies to evaluate catalyst stability and recyclability potential are essential.

The formation of aqueous sugars (e.g., glucose) from the hydrolysis of cellulose can undergo catalytic dehydration to form furan compounds, such as 5-hydroxymethylfurfural (HMF).[26] Although HMF is a versatile platform chemical for the synthesis of added-value chemicals, including 5-hydroxymethylfuran-2-carboxylic acid (HMFCA), 2,5 diformylfuran (DFF), and levulinic acid (LA), it can also be converted into biofuel molecules. Despite its potential, reports on the production of alkanes from HMF using acidic zeolites remain scarce in the literature. Therefore, the remainder of this section is focused on the conversion of C_6 sugars and C_6-sugar
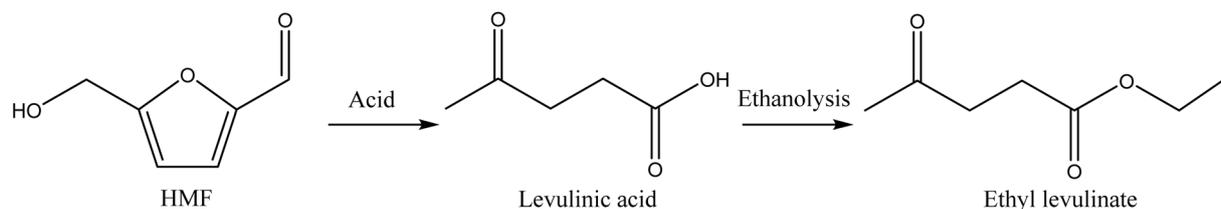

Fig. 4 Reaction pathways for EL production from HMF.

derivatives, such as HMF, into ethyl levuniate (EL) *via* ring-opening and ethanolysis reactions, as shown in Fig. 4.[108] EL is a biofuel of particular interest due to its reduced sulfur content, enhanced flow properties, flash point stability, high lubricity, and high compatibility as a diesel blending component.[112,113]

Zhao *et al.* investigated the conversion of glucose and fructose into EL using a series of supported phosphotungstic acid catalysts, including HPW-β, HPW-Snβ, HPW-H–Y, HPW-H-ZSM-5, and HPW-USY.[102] Among the studied catalysts, HPW-H-ZSM-5 showed the highest catalytic activity for fructose conversion, which resulted in an EL yield of 43.1% at 160 °C for 2 h. However, the authors did not clearly elucidate which physiochemical properties of HPW-H-ZSM-5 were responsible for its superior catalytic activity. Kaewmuangphet *et al.* investigated the activity of propyl sulfonic acid-functionalized zeolites (H–Y, H-ZSM-5, and H–β) for glucose conversion to EL. Among the studied catalysts, H–Y resulted in the highest EL yield of 17.3%. The enhanced activity of H–Y was attributed to its interconnected sodalite cages, which are connected through hexagonal prisms, forming a pore defined by a 12-membered ring that enhanced substrate accessability.[114] When H–Y was functionalized with propyl sulfonic acid to increase Brønsted acidity, an increase in EL yield from 17.3% to 25.1% was observed. Wang *et al.* also investigated the conversion of glucose into 5-ethoxymethylfurfural (EMF) using ultra-stable USY in an ethanol/tetrahydrofuran (THF) system.[103] A glucose conversion of 98% and an EMF yield of 42% were obtained at 200 °C and 10 min. Although high EMF yields were obtained, EL was identified as the main EMF degradation product. The formation of EL occurs through an intermediate product (*i.e.*, 2-furaldehydediethylacetal), and mechanistically, EL production originates from the nucleophilic addition reaction between the carbonyl group of EMF and ethanol.[115] Kinetic studies showed that the conversion of EMF to EL has the highest apparent E_a (~97 kJ mol^{-1}), which explains the limited EMF to EL conversion. DFT studies showed that the presence of THF as a co-solvent hampers the EL production, as THF increases the LUMO (Lowest Unoccupied Molecular Orbital) energy of EMF, which reduces the susceptibility of EMF to be nucleophilically attacked by ethanol.[103]

Compared to other heterogeneous and homogeneous catalysts, zeolites have been shown to have lower activity for EL formation from C$_6$-sugars. Saravanamurugan and Riisager investigated the catalytic activity of various zeolites (H-ZMS-5, H–Y, H–β and H-mordenite), sulfonic acid functionalized SBA-15 (SO$_3$H-SBA-15), and sulfated zirconia for the production of EL.[106] Their study showed that mesoporous SO$_3$H-SBA-15 was highly active and selective, outperforming zeolite and zirconia catalysts, reaching a maximum EL yield of 57% from fructose at 140 °C for 24 h. The superior activity of SO$_3$H-SBA-15 was attributed to its large mesoporous channels combined with strong sulfonic acid groups, which minimized the mass transfer limitations that hamper the dehydration of fructose to HMF, etherification of HMF, and rehydration of the HMF-ether to form EL.[106] Xu *et al.* also compared the catalytic activity of USY zeolite with H$_2$SO$_4$ for glucose conversion into EL.[104] While 1.0 wt% H$_2$SO$_4$ resulted in an EL yield of 48% at 180 °C for 30 min, the USY zeolite led to a similar EL yield at 180 °C, but

required a reaction time of 2 h. This suggests slower reaction kinetics when zeolites were used. Chang *et al.* reported that the combination of low concentrations of H$_2$SO$_4$ and USY constitutes an effective catalytic system for the production of EL from glucose.[105] The mixed catalytic system composed of 0.1% H$_2$SO$_4$ and 2 wt% USY resulted in an EL yield of 51.5 mol%. This increased activity was attributed to the synergetic effects of USY and H$_2$SO$_4$. While USY is more active in converting glucose into EMF, H$_2$SO$_4$ catalyzes ethanolysis of EMF into EL and minimizes mass transfer limitations inherent to solid–liquid reactions.

Chithra and Darbha investigated the activity of parental (HZSM-5), desilicated (DZSM-5) and hierarchical ZSM-5 (MZSM-5) zeolite catalysts to produce EL from HMF at 140 °C for 12 h.[108] Among the studied catalysts, MZSM-5 resulted in the highest conversion of HMF (66%) and highest selectivity to EL (50%) relative to HZSM-5 (HMF conversion of 62% and 7% EL selectivity) and DZSM-5 (HMF conversion of 40% and 14% EL selectivity). Despite its lower acidity (0.55 mmol g^{-1}), the high activity of MZSM-5 was attributed to its intracrystalline mesoporosity, which enhanced the diffusion of bulk EMF intermediates to active sites. The enhanced mass transport in MZSM-5 resulted in a substantially lower apparent activation energy (E_a) of 32.6 kJ mol^{-1}. In contrast, microporous HZSM-5 limited EMF access, which enhanced EMF formation over EL. In the case of DZSM-5, the formation of intercrystalline mesopores led to reduced catalytic activity. The motivation to use hierarchical zeolites lies in minimizing the diffusion constraints inherent to microporous H-ZSM-5, which limits the access of bulky molecules to active sites.

It has been reported that acidic zeolites also catalyze the direct esterification of levulinic acid. Structural and textural properties, including surface area, porosity and acid site access, enable the fine-tuning of catalyst properties to enhance EL yield.[116] For example, desilicated H-ZSM-5 with optimized acidity and porosity achieved 95% LA conversion at 120 °C for 7 h.[110] However, relatively high temperatures and long reaction times were required due to the lower acid strength of the desilicated H-ZSM-5. Similar LA conversions were obtained using 15% dodecatungstophosphoric acid on desilicated H-ZSM-5 at 80 °C for 4 h.[111] High dodecatungstophosphoric acid loadings were required to increase the Brønsted/Lewis ratio, but loadings above 15% resulted in undesired side reactions, such as ether formation and ethanol dehydration.[111] Apart from acidity, the LA esterification into EL by zeolites is highly influenced by pore structure and acid site accessibility. Mesoporous zeolites (*e.g.*, micro-*meso*-HZ-5) reached 95% LA conversion at 130 °C for 300 min, whereas microporous H–β led to only 40% levulinic acid conversion at the same reaction conditions.[109,110]

3.3. Hemicellulose and its intermediates

Hemicellulose represents the second-most available lignocellulosic polymer, after cellulose.[117] In most hardwoods and grasses, xylan, a heteropolysaccharide primarily composed of β-1,4-linked xylose residues, is often found as the predominant form of hemicellulose.[118] The dehydration of xylose can produce

Table 2 Overview of the zeolite-based processes used to convert xylan and xylan-derived compounds into hydrocarbon fuels

Feedstock	Reaction conditions	Catalytic systems	Solvent	Reactor type	Product yield and selectivity	Ref.
Xylan	190 °C, 24 h, 6 MPa H_2	Ir–ReO$_x$/SiO$_2$	n-dodecane/water	Fixed-bed	Xylan conversion: >95%; n-pentane yield: 70%	123
Xylan	200 °C, 5 h	Zr–β + H_2SO_4	Ethanol	Batch	EL yield: 21.5%	127
Xylose	170 °C, 3 h, Ar atmosphere	0.9 wt% Pt/USY	Water	Batch	Xylose conversion: >94.7%; total hydrocarbon yield: 0.8 %C, C_3–C_5 olefin selectivity: 90.7 %C	90
Xylose	200 °C, 5 h	10% Zr/H–β	Ethanol	Batch	EL yield: 40.3%	127
Furfural	150 °C, 24 h	HPMo/Zr-MCM-41	Isopropanol	Batch	Furfural conversion: 99%; isopropyl levulinate yield: 80%	128
Furfural	180 °C, 8 h	Zr-SBA-15/H-ZSM-5	Ethanol	Batch	Furfural conversion: 100%; EL yield: 55%	129
Furfuryl alcohol	125 °C, 0.2 $g_{furfuryl\ alcohol}\ g_{cat}^{-1}\ h^{-1}$	H-ZSM-5	Ethanol	Semi-batch	Furfuryl alcohol conversion: >90%; EL yield: 80 mol%	130
Furfuryl alcohol	140 °C, 4 h	Hierarchical-HZ-5	Ethanol	Batch	Furfuryl alcohol conversion: ~100%; EL yield: 73%	131
Xylitol	240 °C, 4 h, 4 MPa, 500 mL min^{-1} H_2 flow	2 wt% Pt/H-ZSM-5	Water	Batch	Xylitol conversion: 97%, pentane selectivity: 77%	125
Xylitol	240 °C, 4 h, 4 MPa, 500 mL min^{-1} H_2 flow	2 wt% Ni/H-ZSM-5	Water	Batch	Xylitol conversion: > 94%; maximum pentane yield: 91%	124
Xylitol	425 °C, 1.0 h^{-1} weight hourly space velocity	ZSM-5 -WS (28)	—	Fixed-bed	Xylitol conversion: 96%; pentane selectivity: 51%	107

furfural, which can be used as a building block to produce longer carbon fuel precursors.[119,120] Furfural and other lignocellulosic biomass-derivative compounds, such as 2-MF and cyclopentanone, can undergo carbon–carbon coupling reactions, such as aldol condensation[121] and HAA[122] reactions to increase the carbon number in the hydrocarbon precursors, which can then be upgraded to produce jet-fuel range alkanes.[14,78]

In contrast with the extensive body of literature on the catalytic transformation of cellulose, studies on the direct transformation of hemicelluloses into alkanes over zeolite-based catalysts remain scarce (Table 2). To date, a single study has been identified in this field. Liu *et al.* reported the selective conversion of xylan into *n*-pentane over Ir–ReO$_x$/SiO$_2$ combined with H-ZSM-5 + H_2SO_4.[123] The authors found a 70% yield in *n*-pentane at 190 °C for 24 h. Through catalyst stability tests, it was shown that the catalyst remained stable during three consecutive runs as the conversion of xylan and *n*-pentane yield were maintained above 97% and 66%, respectively.[123] Although hemicelluloses can be directly converted into hydrocarbon fuels, like cellulose, using zeolites, the few reports published in the literature have focused on the conversion of hemicellulose-derived compounds, such as xylose and xylitol. Ogo *et al.* studied the conversion of xylose into C_3 and C_4 hydrocarbons using Pt/USY zeolite as the catalyst.[90] They reported a xylose conversion of 94.7% and a total hydrocarbon yield of less than 1% at 170 °C for 3 h. However, it should be noted that the authors used xylose as a substrate primarily to investigate the reaction intermediates involved in the catalytic transformation of lignocellulosic carbohydrates into hydrocarbons, rather than to optimize the hydrocarbon yield from xylose.

The stoichiometry of pentane formation from xylitol involves the xylitol reduction to pentane and aqueous phase reforming of xylitol into hydrogen and CO_2, as shown in eqn (2) and (3).[124]

$$C_5H_{12}O_5 + 5H_2 \rightarrow C_5H_{12} + 5H_2O \tag{2}$$

$$C_5H_{12}O_5 + 5H_2O \rightarrow 5CO_2 + 11H_2 \tag{3}$$
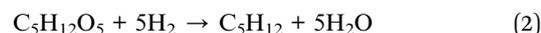
The produced hydrogen can be used to supply H_2 for the reduction reaction. The reaction mechanism for the aqueous-phase reforming of xylitol into pentane over bifunctional catalysts has been proposed and is shown in Fig. 5.

Jiang *et al.* reported that the mechanism involves several steps, including (1) hydrogenation reactions over the metal sites, (2) dehydration on acid sites leading to C–O bond cleavage, (3) decarbonylation reactions over metal sites leading to C–C linkage cleavage, and (4) aldol condensation on acid sites leading to C–C bond formation.[125] Other thermodynamically favored reactions, such as methanation, water-gas shift (WGS), and Fischer–Tropsch (FT) synthesis, can occur simultaneously. Specifically, xylitol is subjected to intermolecular dehydration, leading to the formation of intermediates (*e.g.* alcohols, cyclic ethers and ketones). These species can follow two main routes: one involves cycling dehydration/hydrogenation reactions to produce pentane, while the other proceeds through decarbonylation, producing CO and light oxygenated compounds. Further dehydration and hydrogenation of the lighter compounds result in the formation of C_1–C_4 alkanes. Simultaneously, some linear alkanes undergo isomerization to form branched isoparaffins. The CO released during decarbonylation can be further converted to CO_2 *via* WGS reaction. In addition, heavier alkanes (*i.e.*, hexane) can be produced through C–C coupling reactions (aldol condensation) on acid sites.
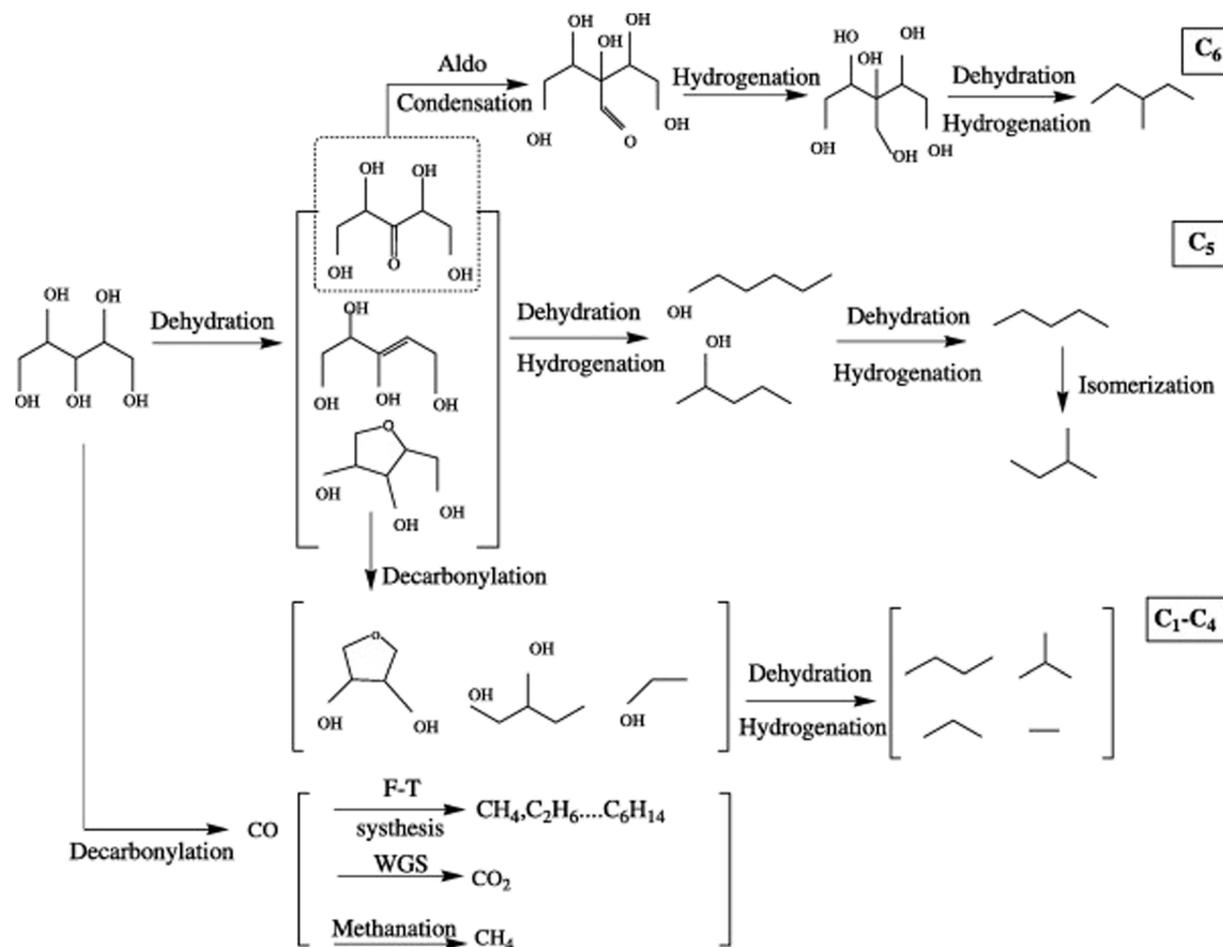
Fig. 5 Proposed reaction pathways for the production of alkanes from xylitol over bifunctional catalysts. Reprinted from ref. 125 with permission from [Elsevier], copyright [2012].

Jiang *et al.* reported the conversion of xylitol into pentane using H-ZSM-5 loaded with Ni.[124] The authors found that the highest pentane yield of 91% was found when 2 wt% Ni/H-ZSM-5 was used at 240 °C and 4 MPa H_2 pressure for 4 h. While xylitol conversion did not change with an increase in Ni loading (from 2 to 4%), a decrease in pentane selectivity from 95 to 60% as C_1–C_4 alkane formation increased. Also, the reported findings suggest that weak acid sites promoted dehydration, while strong acid sites facilitated isomerization and cracking.[125] The authors also tested the recyclability of the 2 wt% Ni/H-ZSM-5 and found that it deactivates significantly by the 5th recycling run due to partial dealumination during reaction. The same group also investigated the impact of metal type loaded (either Pt or Ni) on H-ZSM-5 on the aqueous-phase reforming of xylitol into pentane.[125] Increasing both metal loadings up to 3 wt% (*i.e.* 3% Pt/H-ZSM-5 and 3% Ni/H-ZSM-5) resulted in an enhanced xylitol conversion and pentane selectivity, but a further increase to 5 wt% led to a decrease in pentane selectivity due to enhanced C–C bond cleavage. At 240 °C and 4 MPa, both catalysts with 2 wt% metal loading obtained similar xylitol conversion, but Ni/HZSM-5 showed a superior pentane selectivity of 95% compared to 58% obtained with Pt/HZSM-5. This indicates

that Ni favors pentane formation, while Pt promotes C–C cleavage, leading to lighter alkanes (*e.g.* C_1–C_4). Optimizing the metal loading is critical as it alters the balance between hydrogenation and C–C cleavage reactions, thus affecting alkane selectivity. Also, the authors noted that increased metal loading results in a higher metal/acid ratio, which could lead to a higher rate of C–C linkage cleavage relative to hydrogenation on metal sites, which resulted in lower pentane selectivity.

Beyond their application in the production of alkanes, zeolites have been used in the production of EL from C_5 sugars and C_5 sugar-derived compounds, such as furfural and furfuryl alcohol. For example, C_5 sugars, such as xylose, can undergo a series of reactions, including dehydration, transfer hydrogenation and ethanolysis (Fig. 6).[126]

Recently, Kaewmuangphet *et al.* studied the production of EL from different substrates (xylan and xylose) using Zr–β catalysts and ethanol as a hydrogen donor.[127] The incorporation of ZrO_2 onto β-zeolite enhanced the conversion of xylose into furfural (*via* dehydration), furfural into furfuryl alcohol (*via* hydrogenation) and furfuryl alcohol into EL (*via* ethanolysis). Through this multi-step process, Zr–β showed high activity for EL production, reaching yields up to 40% from xylose. However,
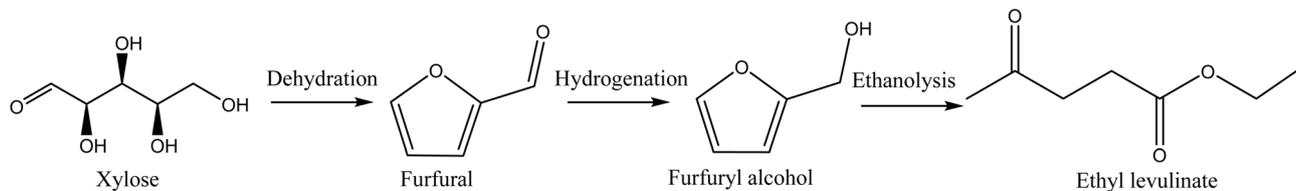
Fig. 6 Reaction pathways to convert xylose into EL.

significantly lower EL yield (∼1.8%) was observed when xylan was used as the substrate. The low EL yield was attributed to the low surface acidity of the catalyst, which was insufficient to promote ethanolysis/hydrolysis of the polymer.[127] The addition of a low concentration of H_2SO_4 increased the EL yield to 52.9%, but the use of even small amounts of homogeneous acid introduces additional downstream steps. Optimization of the reaction conditions and/or more acidic solid catalysts should be developed to eliminate the need for additional homogeneous acids. Pen *et al.* synthesized a zirconia-zeolite-supported heteropoly acid (HPMo(20)/Zr-MCM-41), which was designed to provide tunable Lewis and Brønsted acid sites required for the one-pot conversion of furfural into alkyl levulinates in the presence of isopropanol as both hydrogen donor and solvent.[128] Hydrogenation was mainly catalyzed by Lewis acid sites, while alcoholysis occurred mainly at Brønsted acid sites. The selectivity toward alkyl levulinate was strongly dependent upon the distribution of Brønsted and Lewis acid sites. HPMo(20)/Zr-MCM-41 showed high activity resulting in ∼80% isopropyl levulinate and ∼99% furfural conversion at 150 °C for 24 h. The catalyst showed high stability and reusability, resulting in high activity for at least five cycles.[128] Tang *et al.* further studied the synergistic role of Lewis and Brønsted acid sites in the conversion of furfural into EL.[129] Zr-SBA-15 was used as a Lewis acid catalyst and ZSM-5 was used as a Brønsted catalyst to catalyze the conversion of furfural into furfuryl alcohol and the ethanolysis reaction of furfuryl alcohol to EL, respectively. After optimization of the acidity ratio, a maximum EL yield of 55% was obtained at a B/L molar ratio of 0.074 and at 180 °C for 8 h.

This represents a significant improvement as the obtained EL yield is almost two times higher than the yield achieved when Zr-SBA-15 was used as the Lewis acid catalyst alone. In comparison with W–ZrO$_2$ and phosphotungstic acid, ZSM-5 was the only Brønsted catalyst that contributed to the observed synergetic effect, attributed to its unique pore structure and hydrophobic properties, which minimize polymerization side reactions. However, high Brønsted acidity is undesirable as it enhances side reactions, such as polymerization of furfural and furfuryl alcohol.[129] Lange *et al.* evaluated the catalytic conversion of furfuryl alcohol into EL using macroreticular resins, gel resins, and zeolites as alternatives to H_2SO_4.[130] Catalyst activity was correlated with acid strength and accessibility of the acid sites, which resulted in an overall activity decrease in the order of H_2SO_4, macroreticular resins, gel resins and zeolites. Among the studied zeolites (ZSM-5, ZSM-12, ZSM-23, β, mordenite and Y), H-ZSM-5 resulted in the highest EL yield (80 mol%) at 125 °C, but at a very low feed rate (WHSV = 0.2 $g_{furfuryl\ alcohol}\ g_{cat}^{-1}\ h^{-1}$). When the activity was normalized per mole of acid sites, the H-ZSM-5 activity was similar to that found for macroreticular resins.[130] Also, Bokade and co-workers reported that hierarchical HZ-5 has higher activity toward the conversion of furfuryl alcohol into EL (19% EL yield) relative to conventional zeolites, such as USY (5% EL yield), H–β (8% EL yield) and H-ZSM-5 (13% EL yield), at 100 °C for 2 h.[131] By using a response surface methodology (Box–Behnken experimental design), the authors optimized the reaction conditions resulting in an EL yield of 73% at 140 °C for 4 h.[131] Collectively, these studies show that zeolite-based catalysts can effectively convert C$_5$ sugars and
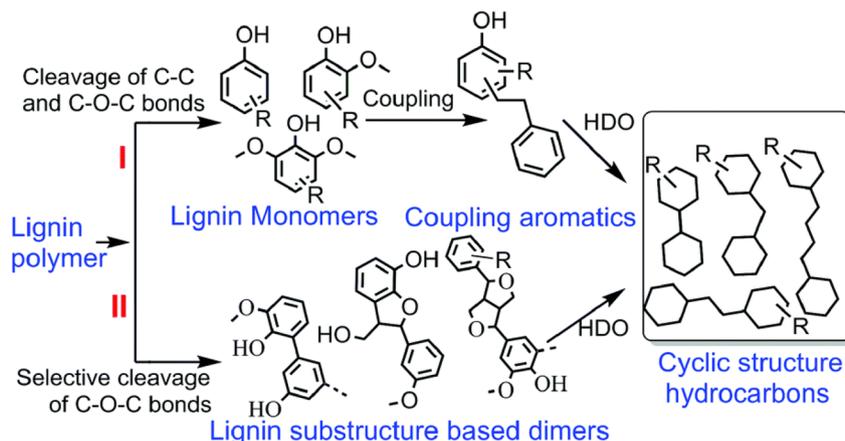

Fig. 7 Proposed routes for depolymerization and HDO of biomass lignin into fuel-like hydrocarbons. Reproduced from ref. 135 with permission from the Royal Society of Chemistry.

Table 3 Overview of the zeolite-based processes used to convert lignin and its intermediates into fuel-like hydrocarbons

Feedstock	Reaction conditions	Catalytic systems	Solvent	Reactor type	Product yield and selectivity	Ref.
Corn stover extracted lignin	250 °C, 4 h, 4 MPa H_2	Ru/Al_2O_3 combined with H-Y	Water	Batch	Lignin conversion: 81.0%; total yield: 21.8^a wt%; product distribution: C_{12}–C_{18} – 84.6% and alkyl cyclohexanes – 89.8%	135
Pine wood extracted lignin	250 °C, 4 h, 4 MPa H_2	Ru/H-Y and Ru-M/HY (M = Fe, Ni, Cu, Zn)	Water	Batch	All Ru–M/H-Y catalysts resulted in lignin conversion: >~80% and total hydrocarbon yield: 26–32 wt%	133
Softwood Kraft lignin	600 °C, 10 min, 500 mL min^{-1} N_2 gas flow	MFI (30), FAU (30), BEA (25), FER (20) and MOR (20)	—	Semi-batch	Zeolites FER and MOR provided the highest heavy oil yield (~30–35%), while MFI, FAU and BEA provided the highest light oil yields (~15–20%)	163
Kraft lignin	320 °C, 24 h, 2 MPa H_2	Co–Zn/Off-Al H-β	Methanol and 1,4-dioxane	Batch	Petroleum ether soluble yield: 81%; heating value: 33.3 MJ kg^{-1}	142
Kraft lignin	290 °C, 2 h, N_2 atmosphere	Ni_1, Zn_1/H-Y_a	Formic acid, methanol and 1,4-dioxane	Batch	Monomer yield: ~38%, liquid product yields: >95%	139
Guaiacol	250 °C, 4 h, 4 MPa H_2	Ru/H-Y and Ru-M/HY (M = Fe, Ni, Cu, Zn)	Water	Batch	All catalysts provided a guaiacol conversion >91%	133
Guaiacol	200 °C, 4 MPa H_2, 120 mL min^{-1} H_2 flow	Ion-exchanged Ru/H-β	—	Continuous flow	Substrate conversion: 17.7%, cyclohexane yield: 14.6%	148
Guaiacol	300 °C, 4 MPa H_2, 200 min	Ion-exchanged Ni/H-β	—	Batch	Substrate conversion: 100%, cyclohexane yield: 76%	153
Guaiacol	260 °C, 2 h, 4 MPa H_2 pressure	Ni_2P/Pt-ZSM-5	Decalin	Batch	Substrate conversion: ~78%; HDO yield: ~95%; cyclohexane selectively: >80%	164
Guaiacol	350 °C, atmospheric pressure, 250 mL min^{-1}	20% Ni/H-USY loaded with 10% Sm or 10% La	—	Fixed-bed	Substrate conversion: ~98% for 10% Sm–20% Ni/HUSY; HDO yield: 7.7% for 10% La–20% Ni/HUSY	156
Guaiacol	180 °C, 100 mL min^{-1}	Ru-HY-60-MI	—	Fixed-bed	Substrate conversion: >99%; cyclohexane yield: 90%	149
Guaiacol	160 °C, 300 min, 3 MPa H_2	Ru/HMCM-22-IN	Dodecane	Batch	Substrate conversion: 40%; cyclohexane selectivity: >95%	146
Guaiacol	230 °C, 4 MPa H_2	11.2 wt% Ni/BEA-IDP	—	Fixed-bed	Substrate conversion: 19.6%; cyclohexane yield: 7.4%	152
Guaiacol	140 °C, 5 h, 5 MPa H_2	Ni/SiO_2, combined with phosphoric acid-modified H–β	Decalin	Batch	Substrate conversion: 99%; cyclohexane yield: 95%	154
Guaiacol	180 °C, 40 min, 1 MPa H_2	Ni-15CoO_x/Hβ-u	n-hexane	Batch	Substrate conversion: ~100%; cyclohexane selectivity: 100%	157
Guaiacol	300 °C, 5 h, 1 MPa N_2	15–20% Ni–Nb_2O_5/H-ZSM-5	Ethanol	Batch	Substrate conversion: ~100%; cyclohexane yield: 48%	162
Guaiacol	250 °C, 2 h, 4 MPa N_2	Pt/HZSM-5 (nanocrystalline, ~40 nm)	n-dodecane	Batch	Substrate conversion: ~100%; cyclohexane yield: ~81%	160
Guaiacol	220 °C, 1 h, 5 MPa N_2	10% Ni/H–β	Hexadecane	Batch	Substrate conversion: ~100%; cyclohexane yield: ~47%	155
4-Ethylguaiacol	230 °C, 3 h, 2 MPa N_2	2D nanosheet catalyst (Ni/HZ5-NS)	n-hexane	Batch	Substrate conversion: ~100%, ethyl-cyclohexane yield: 93%	161

Table 3 (*Contd.*)

Feedstock	Reaction conditions	Catalytic systems	Solvent	Reactor type	Product yield and selectivity	Ref.
Diphenyl ether	250 °C, 2 h, 4 MPa H_2	Ru–Cu/HY	Water	Batch	Substrate conversion: >83%; cyclohexane selectivity: 81.6%	133
Benzyloxy benzene	250 °C, 2 h, 4 MPa H_2	Ru–Cu/HY	Water	Batch	Substrate conversion: >99%; cyclohexane selectivity: 56.1%	133
Benzofuran	250 °C, 2 h, 4 MPa H_2	Ru–Cu/HY	Water	Batch	Substrate conversion: >99%; cyclohexane selectivity: 85.1%	133
Phenol	200 °C, 2 h, 1 MPa H_2	Ni-15CoO$_x$/Hβ-u	n-hexane	Batch	Substrate conversion: ~100%; cyclohexane yield: 100%	157
Phenol	220 °C, 1 h, 5 MPa N_2	10% Ni/H–β	Hexadecane	Batch	Substrate conversion: ~100%; cyclohexane yield: ~42%	155
o-cresol, m-cresol, and p-cresol	200 °C, 2 h, 1 MPa H_2	Ni-15CoO$_x$/Hβ-u	n-hexane	Batch	Substrate conversion: ~100%; cyclohexane yield: 100%	157
Anisol	200 °C, 2.5 h, 3 MPa H_2	Hierarchical nanosponge ZSM-5 (Ni/NPZ)	n-dodecane	Batch	Substrate conversion: >80%; cyclohexane yield: 78.6%	158

^{a} Total yield of the top 23–25 products; values in parentheses correspond to SiO_2/Al_2O_3.

their derivatives to EL. However, fine optimization of the Lewis and Brønsted acid site balance and acid strength of the zeolites is required to maximize EL yields.

4. Conversion of lignin

One of the leading strategies to upgrade lignin into valuable aromatic fuel-like hydrocarbons involves the breaking down its complex structure and the removal of oxygen atoms through depolymerization and deoxygenation reactions (*e.g.*, HDO) (Fig. 7).[132,133] During most HDO reactions, lignin undergoes both C–O–C and C–C linkages cleavage, yielding monomeric products that generally contain 6 to 9 carbon atoms.[134,135] These compounds have the potential to participate in C–C coupling reactions to form long chain hydrocarbons. Alternatively, aliphatic C–C bonds can be maintained (bond dissociation energy ~384 kJ mol^{-1})[136] while C–O linkages (~218–314 KJ mol^{-1})[136] are selectively cleaved during HDO, using lignin intermediates as starting materials.[133,137]

Despite its potential, transforming lignin selectively into valuable aromatic fuel-like hydrocarbons remains a major challenge, largely due to its complex, cross-linked architecture that resists hydrolysis and high reactivity of the intermediates formed during its breakdown.[135,138] Specifically, the stabilization of reaction intermediates during lignin transformation, as well as bond activation, is critical.[139]

Table 3 provides an overview of the diverse reaction conditions and zeolite-based catalysts used to convert lignin and its derivatives. Wang *et al.* investigated the HDO of dilute alkali extracted corn stover lignin, reporting that a catalytic system comprising Ru/Al$_2$O$_3$ and H–Y zeolite at 280 °C under 4 MPa of H$_2$ for 4 h can effectively produce lignin-derived hydrocarbons in the C$_7$–C$_{18}$ range.[135] H–Y zeolite plays a dual role in lignin conversion by inducing C–O bond cleavage to yield monomers and dimers, while also promoting the formation of dimers *via* alkylation and dimerization pathways.[140] Combined with ruthenium-based catalysts, acidic zeolites show strong synergistic effects, significantly enhancing HDO activity. This enables efficient production of cyclohexane from lignin-derived monomers and dimers through hydrogenation of aromatic rings and removal of oxygen-containing groups.[135,140] Inspired by these results, the same research group co-loaded Ru with earth abundant metals (M = Ni, Fe, Cu and Zn) and tested the resulting Ru–M/H–Y catalysts for HDO of softwood lignin.[133] The authors found that Ru–Cu/HY resulted in higher hydrocarbon selectivity compared to other catalysts (*i.e.*, Ru–Ni/H–Y, Ru–Fe/H–Y and Ru–Zn/H–Y), most likely due to the lower activation energy for hydrogen bulk diffusion over Cu relative to other metals.[133,141] However, all bimetallic catalysts provided similar lignin conversion (~80–85%) and hydrocarbon yields (26–32%).

To overcome the challenges associated with using high-pressure H$_2$ for the hydrogenation of lignin, several studies have investigated catalytic transfer hydrogenation (CTH) as an alternative approach. This approach uses organic solvents (*e.g.*, formic acid, isopropanol or their mixtures) as hydrogen donors, thus eliminating the need for external hydrogen gas. For

instance, Zhang *et al.* used a multifunctional Ni–Zn/HY$_a$ catalyst to enhance the *in situ* HDO of Kraft lignin for the production of liquid fuels. The process was conducted in a system composed of formic acid, methanol, and 1,4-dioxane, without the addition of exogenous hydrogen. While methanol and 1,4-dioxane were selected for their ability to dissolve Kraft lignin, formic acid served as a hydrogen donor.[139,142] Ni$_1$,Zn$_1$/HY$_a$ catalyst selectivity converted formic acid into hydrogen for lignin transformation. Ni facilitated the secure anchoring of bidentate carbonate species on Zn sites with an electron-deficient structure. This interaction enhanced the structural transformation of the adsorbed species into monodentate carbonates, which subsequently decomposed to generate active hydrogen species. These hydrogen species were continuously provided for lignin transformation. The synergistic interaction between Lewis acid sites and hydrogenation active sites in Ni$_1$Zn$_1$/H–Y$_a$ significantly improved lignin transformation, while minimizing excessive hydrogenation of aromatic rings.[139] Ni$_1$Zn$_1$/H–Y$_a$ resulted in a liquid product yield higher than 95% and a monomer yield of approximately 38% at 290 °C for 2 h, which are higher than those obtained with H–Y$_a$, Ni–H–Y$_a$, Ni$_3$, Zn$_1$/H–Y$_a$ and Zn/H–Y$_a$. After 24 h, the total liquid product yield and petroleum ether-soluble fraction reached about 92% and 68%, respectively, with Ni$_1$Zn$_1$/H–Y$_a$. Earlier literature shows that Zn plays a critical role in the cleavage of lignin-derived compounds by activating ether bonds and promotes the cleavage of the hydroxyl group from the Cγ position of the β–O–4 ether bond.[143,144] Also, it was found that Zn enhances the adsorption of lignin compounds containing C=O and C–O linkages, thus resulting in enhanced hydrogenation and HDO reactions.[142,145] Based on these findings, Dou *et al.* replaced Al with Zn in H–β zeolite and loaded Co (resulting in a Co–Zn/Off-Al H–β catalyst), due to its acidity and superior adsorption properties, and investigated its effect on the conversion of Kraft lignin into liquid fuels. The authors found that the incorporation of Zn into off-Al H–β enhanced the acidity of the catalyst, resulting in enhanced lignin transformation and condensation, while the loading of Co into off-Al H–β resulted in lower acidity and less lignin transformation and condensation. By optimizing the Co–Zn ratio to 1 : 3, a high yield in petroleum ether compounds of around 55% at 300 °C for 6 h was obtained. A further increase in reaction temperature to 320 °C resulted in a high petroleum ether soluble product yield of ~63%. However, a significant amount of condensation solid yield of ~27% was obtained at 320 °C.[142] The recyclability of the Co–Zn/Off-Al H–β catalyst was investigated through a five-cycle conversion experiment performed at 300 °C for 12 h. After three cycles, the yield of petroleum ether-soluble products decreased from 59.8% to 40.3%, but increased to ~55% after calcination, which indicates that catalyst deactivation was mainly caused by the accumulation of bulky lignin degradation products on the catalyst surface and pores.[142]

4.1.   Lignin intermediates

Guaiacol is one of the most abundant products of lignin transformation processes (*e.g.*, pyrolysis or liquefaction) and has been extensively studied as a model compound for HDO reactions, particularly in the presence of bifunctional catalysts that combine metal sites for hydrogenation and hydrogenolysis with acid sites for the cleavage of C–O bonds.[146] Conceptually, guaiacol contains three different types of C–O bonds (C$_{aryl}$–OH, C$_{alkyl}$–OAr, and C$_{aryl}$–OCH$_3$), which can be cleaved *via* different pathways: (1) hydrogenation followed by dehydration using metal/acid bifunctional catalysts, (2) hydrogenolysis over metal sites, and (3) hydrolysis on acid sites.[146] Guaiacol undergoes HDO resulting in a variety of products, with the product selectivity being impacted by catalyst selection and reaction conditions. These products can range from deoxygenated compounds (*e.g.*, toluene, benzene and cyclohexane) to partially deoxygenated products (*e.g.*, cyclohexanone and phenol).[147]

A wide range of metals have been investigated for the HDO of guaiacol using zeolites as supports. Among the noble metals (*i.e.*, Pt, Ru, Pd and Rh) have been reported to be highly active toward hydrogenation and hydrogenolysis reactions.[148] For instance, Yan *et al.* reported that ion-exchanged Ru-loaded H–β (IX–Ru–H–β), even with low Ru contents (~0.2 wt%) showed 80.6% higher guaiacol conversion and an ~4-fold increase in cyclohexane yield relative to its counterpart synthesized by the incipient wetness impregnation approach (IW–Ru–H–β). This is because Ru species in ion exchange positions have higher activity toward H$_2$ adsorption in comparison to metallic Ru^0 species formed through impregnation.[148] Although ion-exchanged Ru zeolites with low Ru loadings have been shown to be highly active for guaiacol, the resulting guaiacol conversion and cyclohexane yields were still low. Kumar *et al.* developed a Ru-loaded H–Y zeolite catalyst for the HDO of guaiacol under relatively mild conditions (<200 °C and 4 MPa).[149] The authors leveraged a modified incipient wetness impregnation method to synthesize a catalyst with improved acid site uniformity and metal dispersion. This modification involved the addition of acetic acid to generate C$_2$H$_3$O$_2^-$ ions, which stabilize the Ru nanoparticles, resulting in a narrow and uniform nanoparticle size distribution. The resulting catalyst led to a guaiacol conversion of >99% and a cyclohexane yield of 90%. To reduce steric hindrance and enhance access of larger molecules to internal acid sites and metal clusters, He *et al.* developed a catalytic system composed of subnanometric Ru metal clusters (<1.5 nm) encapsulated in H-MCM-22 and its siliceous analog ITQ-1 using an *in situ* ligand-stabilized hydrothermal crystallization approach.[146] The authors tested its performance on the HDO of guaiacol at 160 °C and 3 MPa of H$_2$.[146] Due to its higher surface area, the bifunctional Ru/HMCM-22 catalyst showed high activity and stability for the HDO of guaiacol at 160 °C and 3 MPa H$_2$ pressure. The synergistic effect between Brønsted acid sites and ultrafine and highly dispersed Ru clusters (>86%) was critical to enhance catalytic activity and product selectivity, resulting in a guaiacol conversion of ~40% and a cyclohexane selectivity above 95% at 160 °C, 3 MPa H$_2$ pressure, and 300 min reaction time. Moreover, Ru clusters encapsulated within zeolites show good hydrothermal stability, and no significant metal aggregation or leaching was observed after multiple HDO runs.[146]

Wang *et al.* explored the co-loading of Ru with various earth-abundant metals (*e.g.*, Ni, Fe, Cu and Zn) onto a H–Y zeolite support.[133] They assessed the activity of the resulting Ru–M/H–Y catalysts for HDO of guaiacol, diphenyl ether, benzyloxy benzene and benzofuran as lignin-representative compounds. Using guaiacol as a substrate, the authors found that bimetallic catalysts (*i.e.*, Ru–M/H–Y catalysts) led to higher total yields in hydrocarbons (42–62%) than Ru/H–Y (30%), which shows the high HDO activity of bimetallic catalysts. Among the Ru–M/H–Y catalysts, Ru–Cu/H–Y proved to be the most efficient catalyst, resulting in a total hydrocarbon yield of ∼62%. The enhanced catalytic activity observed for the Ru/Cu/H–Y catalyst was attributed to its high acidity and strong acid sites, high metal dispersion, and superior adsorption capacity for polar fractions (*e.g.*, ether linkages and hydroxyl groups).[133]

Due to their low cost, non-noble metals (*e.g.*, Ni, Fe, Co, Cu, and Mo) are attractive alternatives to Ru. Specifically, Ni-loaded catalysts have been investigated in a variety of applications due to their high activity toward hydrogenation.[150] Ni has a superior capacity to adsorb and activate hydrogen, which facilitates ring hydrogenation and HDO reactions.[147,151] For instance, Yan *et al.* used an ion-exchange-deposition–precipitation method to synthesize a highly dispersed Ni/H–β catalyst with different Ni loadings (6.5 and 11.2 wt%) for the HDO of guaiacol at 230 °C and 4 MPa pressure.[152] While the conversion of guaiacol was not significantly impacted by the synthesis method, the ion-exchanged Ni/H–β catalyst showed a greater cyclohexane formation per surface Ni atom, due to the increased concentration of Ni hydrides on the catalyst surface. Also, the same group investigated the HDO of guaiacol over Ni/H–β and Ni/ZSM-5 catalysts to elucidate the impact of catalyst acidity and Ni structure in the HDO reactions. They reported a 100% guaiacol conversion and a 76% cyclohexane yield with a 15.7 wt% Ni/H–β catalyst at 300 °C.[153] As shown in Fig. 8, their study also proposed two main reaction pathways for the guaiacol HDO catalyzed by Ni loaded on zeolites: (i) a main route in which guaiacol is first hydrogenated 2-methoxy-cyclohexanol over metallic Ni sites, followed by demethylation and dehydroxylation into cyclohexene, methanol and H_2O on acid sites, and hydrogenation of cyclohexene into cyclohexane on metal sites, and (ii) an alternative route occurs when the catalyst shows low hydrogenation activity (*e.g.*, in the absence of Ni) where guaiacol is converted into intermediates (*e.g.*, 1,2-dimethoxybenzene and catechol) on acid sites, after which catechol is rapidly hydrogenated-dehydroxylated into cyclohexane, while 1,2-dimethoxybenzene undergoes slow hydrogenation–demethoxylation reactions to yield cyclohexane.

Wang *et al.* studied the HDO of guaiacol over a catalytic system composed of Ni/SiO_2 with phosphoric acid-modified H–β zeolite, resulting in an almost complete guaiacol conversion and 95% cyclohexane yield at 140 °C and 5 MPa H_2 pressure for 2 h.[154] The modification of H–β with phosphoric acid reduced the concentration of Lewis acid sites while optimizing Brønsted acid sites, thus enhancing the HDO reaction relative to the unmodified H–β catalyst. However, it is important to mention that while the Brønsted acidity of the support is required to convert cyclohexanol into cyclohexane, Ni/SiO_2 was critical to selectively hydrogenate cyclohexene to cyclohexane and guaiacol into cyclohexanol.[154] Margellou *et al.* investigated the HDO of various aromatic model compounds (*e.g.*, phenol, guaiacol, syringol, anisole, *etc.*) using the Ni/H–β catalyst at 220 °C and 5 MPa H_2 pressure for a reaction time of 1 h.[155] The authors reported that 10% Ni/H–β showed good activity and selectivity for the HDO of lignin intermediates, producing suitable molecules for drop-in fuels.

Although the effect of various earth-abundant metals as the main active metal on the HDO of lignin intermediates has been widely investigated, the impact of adding Fe, Ga, Ce, La or Sm as promoters in Ni-loaded bimetallic catalysts for the HDO of guaiacol is not fully understood.[156] Wu *et al.* investigated the effect of adding Fe, Ga, Ce, La or Sm in Ni-loaded H-USY zeolite for the gas-phase HDO of guaiacol. They found that these metal promoters hampered the aggregation of Ni and enhanced its dispersion, leading to higher HDO activities. For example, 20% Ni/H-USY loaded with 10% Sm resulted in the highest guaiacol conversion (∼98%), while 20% Ni/H-USY loaded with 10% La resulted in the highest HDO yield of ∼8% at 350 °C and 4 MPa H_2 pressure.[156] The metal promoters impacted the catalyst reducibility and electron transfer properties, with La and Sm showing moderate interactions with Ni. This interaction enhanced the reduction and dispersion of the active sites compared to strong or weak binding promoters. This interaction resulted in more effective methoxy group removal and aromatic formation. In addition, the authors noted that Ni was the main active site catalyzing the atmospheric HDO of guaiacol, showing its key role in H_2 activation and dissociation.[156]
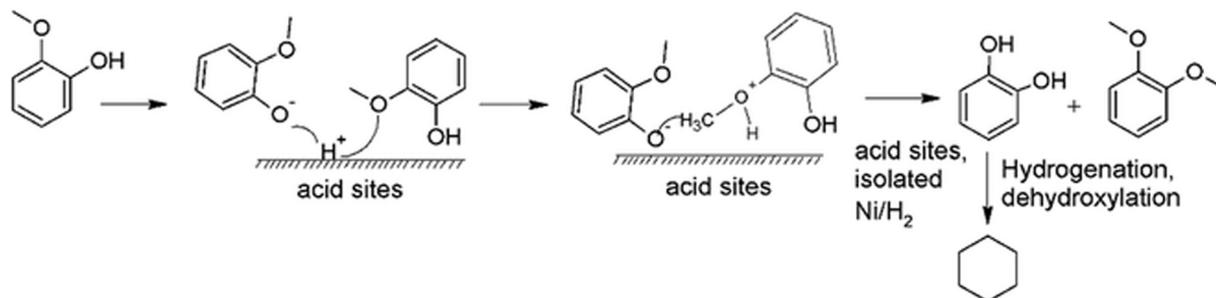

Fig. 8 Proposed reaction pathway for the HDO of guaiacol over the ion-exchanged Ni−H−β catalyst. Reproduced from ref. 153 with permission from the Royal Society of Chemistry.

Also, Fu *et al.* synthesized a series of Ni–CoO$_x$/Hβ-u catalysts by impregnating a H–β molecular sieve modified with urea under mild conditions. These catalysts were tested in guaiacol HDO at 180 °C and 1 MPa H$_2$ pressure.[157] Specifically, the Ni–15CoO$_x$/Hβ-u catalyst achieved 100% guaiacol conversion to cyclohexane with 100% selectivity only after a reaction time of 40 min. This superior catalytic activity was attributed to the enhanced surface area and pore volume, uniformly dispersed metal particles, and defective sites on the CoO$_x$ surface, which enhanced the cleavage of C–O bonds and dehydration reactions. XPS analysis indicated an electronic interaction between Ni and Co, characterized by electron transfer from Co to Ni. This resulted in electron-rich Ni and electron-deficient Co atoms, which in turn enhanced the hydrogenolysis process. The authors suggested that the oxygen atom of the hydroxyl group in the guaiacol molecules likely adsorbs onto a defective CoO$_x$ site, allowing hydrogen ions from Ni and acid sites to cleave the C–O bonds.

In addition to enhancing the interplay between Ni and the zeolite framework, including the modulation of electronic environments of metal active sites through metal–zeolite interactions, it is critical to develop zeolites with both micropores and mesopores with enhanced active site accessibility to promote the diffusion of bulky guaiacol molecules.[158] For example, Xin *et al.* studied the influence of zeolite pore structures on the HDO of guaiacol to benzene.[159] The authors reported that Silicalite-1 (MFI type, with micropore sizes of 5.1–5.6 Å), being smaller than the guaiacol molecule (4.99–6.98 Å), showed exclusive formation of hydrogenolysis products (*e.g.*, benzene and cyclohexanol), while preventing the formation of hydrogenation products (*e.g.*, 2-methoxycyclohexanol). In contrast, larger pore zeolites (*e.g.*, HBEA, HY, and MWW) allowed guaiacol to enter their micropores, promoting both hydrogenolysis and hydrogenation pathways. Wang *et al.* designed a hierarchical nanosponge ZSM-5 loaded with Ni (*i.e.*, Ni/NPZ) to feature both micropores and ordered mesopores and investigated its activity in the HDO of various phenolic compounds (guaiacol, anisol, phenol, *etc.*).[158] The Ni/NPZ catalyst showed a nanosponge morphology with intercrystalline mesopores (∼7 nm), resulting in a higher pore volume and surface area relative to the commercially available microporous ZSM-5 supported Ni catalyst (Ni/CZ) as a control. Also, the Ni/NPZ catalyst showed highly dispersed Ni species and stronger Ni interactions with the zeolite support relative to the Ni/CZ control catalyst. These enhanced properties of Ni/NPZ led to significantly higher catalytic activity and conversion rates for all tested phenolics, enhancing their conversion into cyclohexane. For example, Ni/NPZ achieved an anisole conversion >80% and a cyclohexane yield up to 79% in the HDO of anisole at 200 °C and 3 MPa H$_2$ for 180 min. Also, Duan *et al.* synthesized a series of HZSM-5 zeolites with varying crystallite sizes, Pt/CZ (commercial, ∼1.5 μm, Pt/Z-400 (∼400 nm), Pt/Z-40 (∼40 nm) and Pt/NS-2 (nanosheet, ∼2 nm), loaded with 1 wt% Pt and with similar acidity and Si/Al ratios and investigated their effect on the HDO of guaiacol.[160] The authors found that small crystallite sizes, namely for Pt/Z-40 and Pt/NS-2, resulted in hierarchical zeolites with intracrystalline mesoporosity and enhanced Pt

dispersion. This significantly enhanced the diffusion of bulky guaiacol and intermediates and strengthened the interaction between Pt and the zeolite support, respectively. Although all catalysts resulted in a 100% guaiacol conversion at 250 °C for a reaction time of 60 min, the catalysts with smaller crystallite sizes showed faster conversion rates and higher cyclohexane selectivity relative to the bulk Pt/CZ.[160] In addition, Lin *et al.* synthesized a novel 2-D nanosheet catalyst (Ni-HZ5-NS) with a thickness of 50 nm and tested its performance on the HDO of 4-ethyl guaiacol, a lignin model compound.[161] Characterization showed that Ni-HZ5-NS has thin *b*-direction crystals and broad *a*- and *c*-directions, forming a highly developed (010) crystal plane. It also showed a larger BET surface area and highly dispersed Ni nanoparticles than the commercial HZ5. Under optimal conditions of 230 °C, 2 MPa H$_2$ pressure, and 3 h of reaction time, the 5 wt% Ni/HZ5-NS catalyst achieved 100% conversion of 4-ethylguaiacol and greater than 95% selectivity to ethyl-cycloalkane, specifically yielding 93.2% ethyl-cyclohexane. However, recyclability studies showed that Ni/HZ5-NS exhibited significant deactivation due to Ni particle sintering and agglomeration after the first use. However, the addition of polyvinylpyrrolidone during catalyst preparation effectively prevented Ni agglomeration, allowing the catalyst to be used for three cycles with 4-ethylguaiacol conversion greater than 80%. However, initial recyclability studies showed that Ni/HZ5-NS without additives experienced significant deactivation after the first use, with conversion decreasing to 50% for the second cycle. This deactivation was primarily due to Ni particle sintering and agglomeration. To address this, the addition of polyvinylpyrrolidone (PVP) during catalyst preparation effectively prevented Ni agglomeration, stabilized the metal phase and improved its anti-sintering ability, allowing the catalyst to be used for three cycles with 4-ethylguaiacol conversion remaining higher than 80%.[161] Young-Kwon Park and co-authors explored Ni-impregnated H-ZSM-5 and Nb$_2$O$_5$ catalysts for the HDO of guaiacol at 300 °C, 5 h and 0.1 MPa of N$_2$ in supercritical ethanol.[162] They reported a synergistic effect where Nb$_2$O$_5$ facilitated the cleavage of Ar–O–Me and Ar–OH bonds, converting guaiacol into alkyl phenol, whereas H-ZSM-5 enhances the conversion of these alkyl phenols into aromatics. The incorporation of Ni significantly enhanced aromatic production from 26% with Nb$_2$O$_5$/H-ZSM-5 to 35% for 10% Ni–Nb$_2$O$_5$/H-ZSM-5 and 48% with 15% Ni–Nb$_2$O$_5$/H-ZSM-5.

5. Summary and perspectives

Zeolites play an important role in the catalytic conversion of lignocellulosic biomass components, namely cellulose, hemi-celluloses (xylan), and lignin into drop-in hydrocarbon fuels. However, each of these polymers has distinct structural properties and conversion drawbacks, requiring fine-tuned catalytic approaches to maximize carbon recovery, product selectivity, and product yields.

For cellulose and its intermediates (*e.g.*, glucose, sorbitol, and HMF), zeolites combined with metallic components (*e.g.*, Ir, Pt, and Ni) have been shown to be highly active in catalyzing hydrolysis, hydrogenation, dehydration, isomerization and

HDO reactions needed for cellulose depolymerization and conversion into hydrocarbon fuels. Zeolites, such as H-ZMS-5, H-modernite, H-USY, and H–β, provide Brønsted acidic sites that catalyze hydrolysis, dehydration and/or isomerization, while metal sites enable hydrogenolysis and hydrogenation reactions.[165,166] For zeolites with similar Si/Al ratios, the Brønsted acidity follows the order H-modernite $\approx$ H-ZSM-5 > H–β > H–Y.[167–169] H-modernite, which has similar acidity to H-ZM-5, has a 1-dimensional pore structure and shows a diffusion-limited behavior during catalysis.[169–171] In contrast, the three-dimensional 12-membered-ring (12 MR) pore systems present in zeolites such as H–β and H–Y reduce coke formation/deposition due to the presence of additional diffusion pathways within the framework.[172] For the selective conversion of cellulose and its intermediates into C_5 and C_6 alkanes, which have small molecular kinetic diameters, a strongly acidic zeolite such as H-ZSM-5 is expected to be highly active. The synergy between the metal sites and acidic sites of the zeolite enables the conversion of cellulose and its intermediates into C_5–C_6 with high selectivity.[86,173] For example, recent advances have shown good yields in *n*-hexane using a catalytic system, such as Ir–ReO$_x$/SiO$_2$ with H-ZSM-5. The addition of promoters (*e.g.*, V and Mo) has been reported to further enhance catalyst activity through enhanced hydrogenation and hydrogen spillover effects. However, current operating conditions require long reaction times, high temperatures, and high H_2 pressures, which limit the scalability of the process. Cellulose pretreatments (*e.g.*, ball-milling) can enhance cellulose susceptibility and reduce reaction times, while hierarchical zeolites can improve mass transfer and catalyst stability. Recent studies have shown that the synthesis of hierarchical zeolites by post-synthesis techniques has provided excellent results in the HDO of cellulose intermediates into gasoline-range alkanes.[174] Mesostructuring, also termed surfactant templating, of commercial acidic zeolites has been successful only in zeolites with relatively low framework acid densities, such as H–Y, H–β, and H-mordenite.[72] In contrast, H-ZSM-5, which has a high framework density, usually does not undergo mesostructuring. Thus, the obtained hierarchical H-ZSM-5 does not have a uniform mesopore structure characteristic of a material with a well-defined mesoporous hexagonal arrangement. Although hierarchical ZSM-5 synthesized by desilication or dealumination has increased external surface area, it still presents coke diffusion and redistribution limitations, which contribute to low product selectivity during HDO reactions.[175] In the case of hemicellulose (xylan) and its intermediates (*e.g.*, xylose and xylitol), zeolite-based catalysts have shown potential. However, direct conversion of xylan into hydrocarbon fuels using zeolites is largely underexplored. The few available studies suggest that Ni/H-ZMS-5 can achieve high pentane selectivity from xylitol. Lignin conversion remains challenging due to its highly complex, heterogeneous, and recalcitrant nature. However, several publications report the use of noble metals (Ru and Pt) and Earth-abundant metals (Ni and Cu) supported on acidic zeolites (H–Y, H–β and H-ZSM-5) due to their synergistic effects that enhance lignin depolymerization and HDO activity. To note here that the method of preparation to load the metal on the zeolite, whether ion exchange or incipient wet impregnation, and/or deposition precipitation, is critical to achieve small, well-dispersed nanoparticles. Such control over metal particle size is critical for effective HDO of lignin to produce liquid alkanes, as the synergy between the metal nanoparticles and acidic sites of the zeolite support is the main driving force for effective HDO processing.[176–179] Catalyst optimization, including the addition of promoters (*e.g.*, Zn, Co, La, and Sm), induction of hierarchical porosity, and nanoscale control of metal dispersion, has been critical to improve accessibility of bulky lignin intermediates and enhance catalyst recyclability. The improved recycling and stability of zeolites upon loading of rare earth metals, such as La, Ce, or Sm, is a result of the isomorphous substitution of these elements for the framework Al, which reduces the density of strong acid sites associated with coke formation.[180] However, while strong acid sites are needed to catalyze HDO of lignin and lignin-derived intermediates, the loading of rare earth metals must be carefully optimized, as excessive substitution can significantly reduce catalytic activity.

Despite advances in catalyst design and mechanistic understanding, challenges such as catalyst deactivation, low selectivity control, and limited process scalability still remain. A major challenge is the negative effect of water, produced as a byproduct during HDO reactions, on the structural integrity, performance, and recyclability of zeolite catalysts. Water can cause leaching of framework aluminum, leading to loss of acid sites, low activity and low recyclability, namely during catalyst regeneration–calcination cycles. Studies, namely on zeolite Y, have shown that zeolites can be stabilized against water effects by loading rare earth elements onto the zeolite.[181–184] It has been reported that low rare earth metal loading ($\leq\sim3$ wt% La$_2$O$_3$ equivalent), lighter rare-earth cations, such as La^{3+}, are often located in the sodalite cages in Y-zeolite. La^{3+} exchanges with three Na$^+$ ions and forms La(OH)$_2$ moieties upon calcination and steaming, forming hydrolyzed La–OH species (*e.g.* La(OH)$^{2+}$). These species strongly interact with framework Al–O bonds, which minimizes dealumination and collapse of the zeolite framework under hydrothermal conditions.[181,182,184–186] However, a recent report by Zornes *et al.* claims that the La^{3+} found in the sodalite cages of the Y-zeolites does not prevent further hydrolysis of framework Al, when the LaH–Y zeolite is exposed to moisture, and that more than 50% of the Brønsted acid sites were reduced.[187] Given these contrasting views on stabilizing the framework of Al in Y-zeolite, there is a need for further research and the development of spectroscopic tools to assess the location of rare earth metals and to assess Brønsted acidity *in situ*, with respect to catalyst recycling and stability testing.

Additionally, the presence of ash in the lignocellulosic biomass composition remains another significant challenge. Research is currently ongoing to reduce the ash content of lignocellulosic biomass before it is processed to improve process performance and catalyst recyclability. Although the use of hierarchical zeolites for the conversion of biomass to liquid fuels is still in its infancy, post-synthetic techniques using soft-templating methods have led to the synthesis of hierarchical zeolites with large mesopores. The formation of

mesopores improved coke tolerance and reduced mass transfer limitations during HDO of lignocellulosic biomass and its derived bulky molecules. However, fine-tuned synthesis is required to minimize the risk of collapse of the zeolite structure and reduce catalyst stability. Given the scale of the zeolite industry, future research should focus on the application of hierarchical and water-resistant zeolites for efficient, scalable conversion of lignocellulosic biomass and its derivatives to produce a wide range of liquid fuels, including gasoline, jet fuel, and renewable diesel.

Conflicts of interest

The authors declare no conflicts of interest.

Data availability

No primary research results, software or code have been included and no new data were generated or analyzed as part of this review.

Acknowledgements

References

1 F. REN21 Secretariat Paris, Renewables 2023 Global Status Report Collection, Renewables in Energy Supply, https://www.ren21.net/gsr-2023/, accessed April, 2025.

2 U. S. Department of Energy, U. S. Department of Transportation, U. S. Department of Agriculture. Agency, *SAF Grand Challenge Roadmap: Flight Plan for Sustainable Aviation Fuel*, 2022.

3 B. Dudley, *Report–BP Energy Economics*, London, UK, 2018, vol. 9.

4 R. C. Neves, B. C. Klein, R. J. da Silva, M. C. A. F. Rezende, A. Funke, E. Olivarez-Gómez, A. Bonomi and R. Maciel-Filho, *Renew. Sustain. Energy Rev.*, 2020, **119**, 109607.

5 J. Conti, P. Holtberg, J. Diefenderfer, A. LaRose, J. T. Turnure and L. Westfall, *International Energy Outlook 2016 with Projections to 2040*, USDOE Energy Information Administration (EIA), Washington, DC (United States), 2016.

6 F. Kreith and D. Y. Goswami, *Energy Management and Conservation Handbook*, CRC Press, 2007.

7 P. Fornasiero and M. Graziani, *Renewable Resources and Renewable Energy: a Global Challenge*, CRC press, 2011.

8 J. N. Chheda, G. W. Huber and J. A. Dumesic, *Angew. Chem., Int. Ed.*, 2007, **46**, 7164–7183.

9 A. J. Ragauskas, C. K. Williams, B. H. Davison, G. Britovsek, J. Cairney, C. A. Eckert, W. J. Frederick Jr, J. P. Hallett, D. J. Leak and C. L. Liotta, *Science*, 2006, **311**, 484–489.

10 D. L. Klass, *Biomass for Renewable Energy, Fuels, and Chemicals*, Elsevier, 1998.

11 H. Wang, B. Yang, Q. Zhang and W. Zhu, *Renew. Sustain. Energy Rev.*, 2020, **120**, 109612.

12 N. Pavlenko, *An assessment of the policy options for driving sustainable aviation fuels in the European Union*, ICCT, Washington, DC, USA, 2021.

13 G. W. Huber, S. Iborra and A. Corma, *Chem. Rev.*, 2006, **106**, 4044–4098.

14 M. J. Climent, A. Corma and S. Iborra, *Green Chem.*, 2014, **16**, 516–547.

15 P. H. Galebach, M. Beussman, J. Johnson, T. Fredriksen, C. Wang, M. P. Lanci and G. W. Huber, *ACS Sustain. Chem. Eng.*, 2021, **9**, 2067–2079.

16 A. V. Bridgwater, *Biomass Bioenergy*, 2012, **38**, 68–94.

17 M. Shahabuddin, M. T. Alam, B. B. Krishna, T. Bhaskar and G. Perkins, *Bioresour. Technol.*, 2020, **312**, 123596.

18 E. L. Kunkes, D. A. Simonetti, R. M. West, J. C. Serrano-Ruiz, C. A. Gartner and J. A. Dumesic, *Science*, 2008, **322**, 417–421.

19 Z. Sun, G. Bottari, A. Afanasenko, M. C. Stuart, P. J. Deuss, B. Fridrich and K. Barta, *Nat. Catal.*, 2018, **1**, 82–92.

20 W. Sun, Y. Yan, Y. Wei, J. Ma, Z. Niu and G. Hu, *Nanomaterials*, 2025, **15**, 493.

21 R. Cai, X. Pei, H. Pan, K. Wan, H. Chen, Z. Zhang and Y. Zhang, *Energy Fuels*, 2020, **34**, 11771–11790.

22 S. Soltanian, C. L. Lee and S. S. Lam, *Biofuel Res. J.*, 2020, **7**, 1217–1234.

23 C. Forsberg, B. E. Dale and E. Ingersoll, *ASME Open J. Eng.*, 2024, **3**, 031004.

24 B. E. Dale and S. Kim, *Biorefineries-Industrial Processes and Products: Status Quo and Future Directions*, 2005, pp. 41–66.

25 C. Forsberg and B. Dale, *Can a Nuclear-Assisted Biofuels System Enable Liquid Biofuels as the Economic Low-Carbon Replacement for All Liquid Fossil Fuels and Hydrocarbon Feedstocks and Enable Negative Carbon Emissions?*, Idaho National Laboratory (INL), Idaho Falls, ID (United States), 2022.

26 D. M. Alonso, J. Q. Bond and J. A. Dumesic, *Green Chem.*, 2010, **12**, 1493–1513.

27 H. Wang, B. Zhang, S. Xiu, R. Li and J. Shi, *Curr. Org. Chem.*, 2016, **20**, 2480–2488.

28 T. Renders, G. Van den Bossche, T. Vangeel, K. Van Aelst and B. Sels, *Curr. Opin. Biotechnol.*, 2019, **56**, 193–201.

29 B. Segers, P. Nimmegeers, M. Spiller, G. Tofani, E. J. Grojzdek, E. Dace, T. Kikas, J. M. Marchetti, M. Rajić and G. Yildiz, *RSC Sustain.*, 2024, **2**, 3730–3749.

30 A. U. Buranov and G. Mazza, *Ind. Crop. Prod.*, 2008, **28**, 237–259.

31 A. R. Morais, A. M. da Costa Lopes and R. Bogel-Łukasik, *Chem. Rev.*, 2015, **115**, 3–27.

32 J. Wang, S. Hong, B. Wang, X. Shen, J.-L. Wen and T.-Q. Yuan, *Chem Catal.*, 2023, **3**, 100797.

33 P. C. Rodrigues Pinto, E. A. Borges da Silva and A. r. E. d. Rodrigues, *Ind. Eng. Chem. Res.*, 2011, **50**, 741–748.

34 T. Ennaert, J. Van Aelst, J. Dijkmans, R. De Clercq, W. Schutyser, M. Dusselier, D. Verboekend and B. F. Sels, *Chem. Soc. Rev.*, 2016, **45**, 584–611.

35 Z. Magyarová, M. Králik and T. Soták, *Monatsh. Chem.*, 2023, **154**, 815–835.

36 D. Cole-Hamilton and R. Tooze, in *Catalyst Separation, Recovery and Recycling: Chemistry and Process Design*, Springer, 2006, pp. 1–8.

37 F. Cavani, G. Centi, S. Perathoner and F. Trifirò, *Sustainable Industrial Chemistry: Principles, Tools and Industrial Examples*, John Wiley & Sons, 2009.

38 Q. Sun, N. Wang and J. Yu, *Adv. Mater.*, 2021, **33**, 2104442.

39 Y. Li, L. Li and J. Yu, *Chem*, 2017, **3**, 928–949.

40 J. Čejka, G. Centi, J. Perez-Pariente and W. J. Roth, *Catal. Today*, 2012, **179**, 2–15.

41 *Database of Zeolite Structures*, https://www.iza-structure.org/databases/, accessed September, 2025.

42 J. Yu and R. Xu, *Acc. Chem. Res.*, 2010, **43**, 1195–1204.

43 A.-Y. Lo and F. Taghipour, *Appl. Mater. Today*, 2021, **23**, 101042.

44 C. Martínez and A. Corma, *Coord. Chem. Rev.*, 2011, **255**, 1558–1580.

45 K. Na, M. Choi and R. Ryoo, *Microporous Mesoporous Mater.*, 2013, **166**, 3–19.

46 D. Kerstens, B. Smeyers, J. Van Waeyenberg, Q. Zhang, J. Yu and B. F. Sels, *Adv. Mater.*, 2020, **32**, 2004690.

47 Q. Zou, W. Lin, D. Xu, S. Wu, A. K. Mondal and F. Huang, *Fuel Process. Technol.*, 2022, **237**, 107467.

48 L. G. Possato, T. F. Chaves, W. H. Cassinelli, S. H. Pulcinelli, C. V. Santilli and L. Martins, *Catal. Today*, 2017, **289**, 20–28.

49 G. T. Kadja, R. R. Mukti, I. Nyoman Marsih and I. Ismunandar, *Adv. Mater. Res.*, 2015, **1112**, 201–204.

50 W. Vermeiren and J.-P. Gilson, *Top. Catal.*, 2009, **52**, 1131–1161.

51 C. Perego and A. Bosetti, *Microporous Mesoporous Mater.*, 2011, **144**, 28–39.

52 S. Shao, H. Zhang, D. Shen and R. Xiao, *RSC Adv.*, 2016, **6**, 44313–44320.

53 Y. Wei, T. E. Parmentier, K. P. de Jong and J. Zečević, *Chem. Soc. Rev.*, 2015, **44**, 7234–7261.

54 T. N. Trinh, P. A. Jensen, K. Dam-Johansen, N. O. Knudsen, H. R. Sørensen and S. Hvilsted, *Energy Fuels*, 2013, **27**, 1399–1409.

55 F. Lin, M. Xu, K. K. Ramasamy, Z. Li, J. L. Klinger, J. A. Schaidle and H. Wang, *ACS Catal.*, 2022, **12**, 13555–13599.

56 S. Kim, E. E. Kwon, Y. T. Kim, S. Jung, H. J. Kim, G. W. Huber and J. Lee, *Green Chem.*, 2019, **21**, 3715–3743.

57 K. Stanciakova and B. Weckhuysen, *Trends Chem.*, 2021, **3**, 456–468.

58 L. Zhang, K. Chen, B. Chen, J. L. White and D. E. Resasco, *J. Am. Chem. Soc.*, 2015, **137**, 11810–11819.

59 J. Huo, J.-P. Tessonnier and B. H. Shanks, *ACS Catal.*, 2021, **11**, 5248–5270.

60 Y. Yan, X. Guo, Y. Zhang and Y. Tang, *Catal. Sci. Technol.*, 2015, **5**, 772–785.

61 T. Prasomsri, W. Jiao, S. Z. Weng and J. G. Martinez, *Chem. Commun.*, 2015, **51**, 8900–8911.

62 S. Moon, H.-J. Chae and M. B. Park, *Appl. Catal., A*, 2018, **553**, 15–23.

63 T. Ennaert, J. Geboers, E. Gobechiya, C. M. Courtin, M. Kurttepeli, K. Houthoofd, C. E. Kirschhock, P. C. Magusin, S. Bals and P. A. Jacobs, *ACS Catal.*, 2015, **5**, 754–768.

64 J. Li, X. Li, G. Zhou, W. Wang, C. Wang, S. Komarneni and Y. Wang, *Appl. Catal., A*, 2014, **470**, 115–122.

65 D. P. Serrano, J. Escola and P. Pizarro, *Chem. Soc. Rev.*, 2013, **42**, 4004–4035.

66 R. Li, D. Huang, Z. Wei, Y. Chen, G. Wang, W. Zhou, R. Xiao and W. Xu, *Renew. Sustain. Energy Rev.*, 2025, **207**, 114977.

67 G. Papanikolaou, D. Chillè, S. Perathoner, G. Centi, M. Migliori, G. Giordano and P. Lanzafame, *Microporous Mesoporous Mater.*, 2023, **358**, 112330.

68 J. C. Groen, J. A. Moulijn and J. Pérez-Ramírez, *J. Mater. Chem.*, 2006, **16**, 2121–2131.

69 K. Li, J. Valla and J. Garcia-Martinez, *ChemCatChem*, 2014, **6**, 46–66.

70 S. Mardiana, N. J. Azhari, T. Ilmi and G. T. Kadja, *Fuel*, 2022, **309**, 122119.

71 W. Khan, X. Jia, Z. Wu, J. Choi and A. C. Yip, *Catalysts*, 2019, **9**, 127.

72 J. Pérez-Pariente, M. Sánchez-Sánchez and J. A. Pliego, in *Advancements in Zeolites and Micro-meso Porous Hierarchical Materials*, IGI Global Scientific Publishing, 2025, pp. 315–358.

73 D. P. Serrano, J. A. Melero, G. Morales, J. Iglesias and P. Pizarro, *Catal. Rev.*, 2018, **60**, 1–70.

74 C. Perego, A. Bosetti, M. Ricci and R. Millini, *Energy Fuels*, 2017, **31**, 7721–7733.

75 O. K. Siakpebru, A. Uchagawkar, L. Gurrala, J. Bartlett, P. Adamson, N. Gorschak, A. Hassiba, P. S. Niphadkar, V. V. Bokade and A. R. Morais, *Energy Fuels*, 2024, **38**, 13029–13038.

76 Q. Xia, Z. Chen, Y. Shao, X. Gong, H. Wang, X. Liu, S. F. Parker, X. Han, S. Yang and Y. Wang, *Nat. Commun.*, 2016, **7**, 11162.

77 H.-T. Vu, F. M. Harth and N. Wilde, *Front. Chem.*, 2018, **6**, 143.

78 O. K. Siakpebru, L. Gurrala, A. Uchagawkar, O. Norris, J. Bartlett and A. R. C. Morais, *Ind. Eng. Chem. Res.*, 2025, **64**, 5830–5840.

79 R. Atalla, J. Ellis and L. Schroeder, *J. Wood Chem. Technol.*, 1984, **4**, 465–482.

80 B. O. de Beeck, M. Dusselier, J. Geboers, J. Holsbeek, E. Morré, S. Oswald, L. Giebeler and B. F. Sels, *Energy Environ. Sci.*, 2015, **8**, 230–240.

81 R. Rinaldi and F. Schüth, *ChemSusChem*, 2009, **2**, 1096–1107.

82 L. Jin, W. Li, Q. Liu, L. Ma, C. Hu, A. T. Ogunbiyi, M. Wu and Q. Zhang, *Bioresour. Technol.*, 2020, **297**, 122492.

83 Y. Liu, L. Chen, T. Wang, X. Zhang, J. Long, Q. Zhang and L. Ma, *RSC Adv.*, 2015, **5**, 11649–11657.

84 S. Liu, M. Tamura, Y. Nakagawa and K. Tomishige, *ACS Sustain. Chem. Eng.*, 2014, **2**, 1819–1827.

85 Y. Nakagawa, Y. Shinmi, S. Koso and K. Tomishige, *J. Catal.*, 2010, **272**, 191–194.

86 L. Jin, W. Li, Q. Liu, L. Ma, S. Li, Y. Liu, B. Zhang and Q. Zhang, *Fuel Process. Technol.*, 2019, **196**, 106161.

87 N. S. Date, A. M. Hengne, K.-W. Huang, R. C. Chikate and C. V. Rode, *Green Chem.*, 2018, **20**, 2027–2037.

88 Y. Kato and Y. Sekine, *Catal. Lett.*, 2013, **143**, 418–423.

89 K. Murata, Y. Liu, M. Inaba and I. Takahara, *Catal. Lett.*, 2010, **140**, 8–13.

90 S. Ogo, T. Nishio, H. Sekine, A. Onda and Y. Sekine, *Fuel Process. Technol.*, 2016, **141**, 123–129.

91 S. Ogo, Y. Okuno, H. Sekine, S. Manabe, T. Yabe, A. Onda and Y. Sekine, *ChemistrySelect*, 2017, **2**, 6201–6205.

92 K. Chen, M. Tamura, Z. Yuan, Y. Nakagawa and K. Tomishige, *ChemSusChem*, 2013, **6**, 613–621.

93 E. I. Gürbüz and J. A. Dumesic, *Catalytic Strategies and Chemistries Involved in the Conversion of Sugars to Liquid Transportation Fuels*, 2013.

94 G. W. Huber, R. D. Cortright and J. A. Dumesic, *Angew. Chem., Int. Ed.*, 2004, **43**, 1549–1551.

95 Q. Zhang, K. Qiu, B. Li, T. Jiang, X. Zhang, L. Ma and T. Wang, *Fuel*, 2011, **90**, 3468–3472.

96 C. M. López, Y. Guillén, L. García, L. Gómez and Á. Ramírez, *Catal. Lett.*, 2008, **122**, 267–273.

97 D. Fãrcaşiu and K.-H. Lee, *J. Mol. Catal. A: Chem.*, 2000, **161**, 213–221.

98 Q. Zhang, T. Wang, Y. Xu, Q. Zhang and L. Ma, *Energy Convers. Manag.*, 2014, **77**, 262–268.

99 Y. Weng, S. Qiu, L. Ma, Q. Liu, M. Ding, Q. Zhang, Q. Zhang and T. Wang, *Catalysts*, 2015, **5**, 2147–2160.

100 Y. Weng, S. Qiu, Y. Xu, M. Ding, L. Chen, Q. Zhang, L. Ma and T. Wang, *Energy Convers. Manage.*, 2015, **94**, 95–102.

101 S. Kaewmuangphet, J. S. Samec and D. N. Tungasmita, *J. Clean. Prod.*, 2024, **466**, 142896.

102 S. Zhao, G. Xu, J. Chang, C. Chang, J. Bai, S. Fang and Z. Liu, *BioResources*, 2015, **10**, 2223–2234.

103 S. Wang, Y. Chen, Y. Jia, C. Wang, G. Xu, Y. Jiao, C. He, C. Chang and Q. Guo, *Fuel*, 2022, **326**, 125075.

104 G.-Z. Xu, C. Chang, W.-N. Zhu, B. Li, X.-J. Ma and F.-G. Du, *Chem. Pap.*, 2013, **67**, 1355–1363.

105 C. Chang, G. Xu, W. Zhu, J. Bai and S. Fang, *Fuel*, 2015, **140**, 365–370.

106 S. Saravanamurugan and A. Riisager, *Catal. Commun.*, 2012, **17**, 71–75.

107 S. Narayanan, J. Judith Vijaya, S. Sivasanker, T. Sankaranarayanan, C. Ragupathi, L. John Kennedy, R. Jothiramalingam, H. A. Al-Lohedan and A. M. Tawfeek, *React. Kinet. Mech. Catal.*, 2017, **122**, 247–257.

108 P. Chithra and S. Darbha, *Catal. Commun.*, 2020, **140**, 105998.

109 C. Patil, P. Niphadkar, V. Bokade and P. Joshi, *Catal. Commun.*, 2014, **43**, 188–191.

110 K. Y. Nandiwale, P. S. Niphadkar, S. S. Deshpande and V. V. Bokade, *J. Chem. Technol. Biotechnol.*, 2014, **89**, 1507–1515.

111 K. Y. Nandiwale, S. K. Sonar, P. S. Niphadkar, P. N. Joshi, S. S. Deshpande, V. S. Patil and V. V. Bokade, *Appl. Catal., A*, 2013, **460**, 90–98.

112 A. Démolis, N. Essayem and F. Rataboul, *ACS Sustain. Chem. Eng.*, 2014, **2**, 1338–1352.

113 E. Christensen, A. Williams, S. Paul, S. Burton and R. L. McCormick, *Energy Fuels*, 2011, **25**, 5422–5428.

114 Q. Yu, W. Zhang, J. Li, W. Liu, Y. Wang, W. Chu, X. Zhang, L. Xu, X. Zhu and X. Li, *Microporous Mesoporous Mater.*, 2023, **355**, 112570.

115 S. Wang, Y. Chen, Y. Jia, G. Xu, C. Chang, Q. Guo, H. Tao, C. Zou and K. Li, *Phys. Chem. Chem. Phys.*, 2021, **23**, 19729–19739.

116 E. Ahmad, M. I. Alam, K. Pant and M. A. Haider, *Green Chem.*, 2016, **18**, 4804–4823.

117 S. Dumitriu, *Polysaccharides: Structural Diversity and Functional Versatility*, CRC press, 2004.

118 S. Dutta, S. De, B. Saha and M. I. Alam, *Catal. Sci. Technol.*, 2012, **2**, 2025–2036.

119 G. Li, N. Li, J. Yang, L. Li, A. Wang, X. Wang, Y. Cong and T. Zhang, *Green Chem.*, 2014, **16**, 594–599.

120 S. Dutta, A. Bohre, W. Zheng, G. R. Jenness, M. Núñez, B. Saha and D. G. Vlachos, *ACS Catal.*, 2017, **7**, 3905–3915.

121 J. Yang, N. Li, G. Li, W. Wang, A. Wang, X. Wang, Y. Cong and T. Zhang, *Chem. Commun.*, 2014, **50**, 2572–2574.

122 G. Li, N. Li, Z. Wang, C. Li, A. Wang, X. Wang, Y. Cong and T. Zhang, *ChemSusChem*, 2012, **5**, 1958–1966.

123 S. Liu, Y. Okuyama, M. Tamura, Y. Nakagawa, A. Imai and K. Tomishige, *Green Chem.*, 2016, **18**, 165–175.

124 T. Jiang, Q. Zhang, T.-J. Wang, Q. Zhang and L.-L. Ma, *Energy Convers. Manag.*, 2012, **59**, 58–65.

125 T. Jiang, T. Wang, L. Ma, Y. Li, Q. Zhang and X. Zhang, *Appl. Energy*, 2012, **90**, 51–57.

126 M. Wang, L. Peng, X. Gao, L. He and J. Zhang, *Sustain. Energy Fuels*, 2020, **4**, 1383–1395.

127 S. Kaewmuangphet, S. Lohanut, J. S. Samec and D. N. Tungasmita, *Bioresour. Technol.*, 2025, 132840.

128 L. Peng, X. Gao, Y. Liu, J. Zhang and L. He, *Energy Fuels*, 2021, **35**, 4182–4190.

129 K. Tang, S. Xie, G. R. Cofield, X. Yang, E. Tian and H. Lin, *Energy Technol.*, 2018, **6**, 1826–1831.

130 J. P. Lange, W. D. van de Graaf and R. J. Haan, *ChemSusChem*, 2009, **2**, 437–441.

131 K. Y. Nandiwale, A. M. Pande and V. V. Bokade, *RSC Adv.*, 2015, **5**, 79224–79231.

132 Z. Luo, Y. Wang, M. He and C. Zhao, *Green Chem.*, 2016, **18**, 433–441.

133 H. Wang, H. Ruan, M. Feng, Y. Qin, H. Job, L. Luo, C. Wang, M. H. Engelhard, E. Kuhn and X. Chen, *ChemSusChem*, 2017, **10**, 1846–1856.

134 R. Ma, W. Hao, X. Ma, Y. Tian and Y. Li, *Angew. Chem.*, 2014, **126**, 7438–7443.

135 H. Wang, H. Ruan, H. Pei, H. Wang, X. Chen, M. P. Tucker, J. R. Cort and B. Yang, *Green Chem.*, 2015, **17**, 5131–5135.

136 J. He, C. Zhao, D. Mei and J. A. Lercher, *J. Catal.*, 2014, **309**, 280–290.

137 C. Zhao and J. A. Lercher, *ChemCatChem*, 2012, **4**, 64–68.

138 P. J. Deuss, M. Scott, F. Tran, N. J. Westwood, J. G. de Vries and K. Barta, *J. Am. Chem. Soc.*, 2015, **137**, 7456–7467.

139 X. Zhang, Y. Jiang, W. Li, L. Zhu and L. Wang, *Energy Convers. Manage.*, 2024, **302**, 118144.

140 J. S. Yoon, Y. Lee, J. Ryu, Y.-A. Kim, E. D. Park, J.-W. Choi, J.-M. Ha, D. J. Suh and H. Lee, *Appl. Catal., B*, 2013, **142**, 668–676.

141 P. Ferrin, S. Kandoi, A. U. Nilekar and M. Mavrikakis, *Surf. Sci.*, 2012, **606**, 679–689.

142 X. Dou, X. Jiang, W. Li, C. Zhu, Q. Liu, Q. Lu, X. Zheng, H.-m. Chang and H. Jameel, *Appl. Catal., B*, 2020, **268**, 118429.

143 T. H. Parsell, B. C. Owen, I. Klein, T. M. Jarrell, C. L. Marcum, L. J. Haupert, L. M. Amundson, H. I. Kenttämaa, F. Ribeiro and J. T. Miller, *Chem. Sci.*, 2013, **4**, 806–813.

144 I. Klein, C. Marcum, H. Kenttämaa and M. M. Abu-Omar, *Green Chem.*, 2016, **18**, 2399–2405.

145 E. Rodrigues, A. J. Marchi, C. R. Apesteguia and J. Bueno, *Appl. Catal., A*, 2005, **294**, 197–207.

146 P. He, Q. Yi, H. Geng, Y. Shao, M. Liu, Z. Wu, W. Luo, Y. Liu and V. Valtchev, *ACS Catal.*, 2022, **12**, 14717–14726.

147 S. Valizadeh, B. Valizadeh, J. Lee and Y. K. Park, *ChemCatChem*, 2025, **17**, e202401390.

148 P. Yan, E. Kennedy and M. Stockenhuber, *J. Catal.*, 2021, **396**, 157–165.

149 A. Kumar, A. Kumar, D. M. Santosa, H. Wang, P. Zuo, C. Wang, A. Mittal, R. Gieleciak, D. P. Klein and M. J. Manto, *Appl. Catal., A*, 2024, **676**, 119649.

150 M. Lin, D. Jiang, Y. Yan, L. Zhan, X. Song, R. Li and Y. Wu, *Bioresour. Technol.*, 2024, **413**, 131478.

151 X. Zhang, W. Tang, Q. Zhang, T. Wang and L. Ma, *Appl. Energy*, 2018, **227**, 73–79.

152 P. Yan, J. Mensah, A. Adesina, E. Kennedy and M. Stockenhuber, *Appl. Catal., B*, 2020, **267**, 118690.

153 P. Yan, M. M.-J. Li, E. Kennedy, A. Adesina, G. Zhao, A. Setiawan and M. Stockenhuber, *Catal. Sci. Technol.*, 2020, **10**, 810–825.

154 X. Wang, Y. Lv, S. Zhu, X. Wang and C. Deng, *Catalysts*, 2021, **11**, 962.

155 A. G. Margellou, F. F. Zormpa, D. Karfaridis, S. A. Karakoulia and K. S. Triantafyllidis, *Catalysts*, 2025, **15**, 48.

156 Y. Wu, X. Xu, Y. Sun, E. Jiang, X. Fan, R. Tu and J. Wang, *Renewable Energy*, 2020, **152**, 1380–1390.

157 Z.-P. Fu, Q.-J. Zhou, Y.-P. Zhao, Y.-F. Wu, F.-J. Liu, M. Zhong, J. Li, J. Liang and J.-P. Cao, *Mol. Catal.*, 2025, **576**, 114932.

158 H. Wang, S.-a. Wang, L. Guo, C. Qiao and Y. Tian, *Chem. Eng. J.*, 2023, **455**, 140647.

159 Y. Xin, Z. Zheng, Z. Luo, C. Jiang, S. Gao, Z. Wang and C. Zhao, *Green Energy Environ.*, 2022, **7**, 1014–1023.

160 H. Duan, Y. Tian, S. Gong, B. Zhang, Z. Lu, Y. Xia, Y. Shi and C. Qiao, *Nanomaterials*, 2020, **10**, 2246.

161 F. Lin, Y. Ma, Y. Sun, Z. Song, X. Men, Y. Wu, Y. Zhu, T. Gao and Y. Zhong, *Renewable Energy*, 2022, **189**, 1278–1291.

162 A. Kumar, Y. Khani, C. H. Ko, J. Jae, A. Banerjee, T. Bhaskar and Y.-K. Park, *ACS Sustain. Chem. Eng.*, 2024, **12**, 10786–10804.

163 H. Ben and A. J. Ragauskas, *RSC Adv.*, 2012, **2**, 12892–12898.

164 S. Gutiérrez-Rubio, A. Berenguer, J. Přech, M. Opanasenko, C. Ochoa-Hernández, P. Pizarro, J. Čejka, D. P. Serrano, J. M. Coronado and I. Moreno, *Catal. Today*, 2020, **345**, 48–58.

165 J. Weitkamp, *Solid State Ionics*, 2000, **131**, 175–188.

166 T. Li, S.-H. Chung, S. Nastase, A. Galilea, Y. Wang, I. Mukhambetov, M. Zaarour, J. C. N. de Miguel, J. Cazemier and A. Dokania, *Chem Catal.*, 2023, **3**, 100540.

167 D. Parrillo and R. Gorte, *J. Phys. Chem.*, 1993, **97**, 8786–8792.

168 M. Crocker, R. Herold, M. Sonnemans, C. Emeis, A. Wilson and J. Van Der Moolen, *J. Phys. Chem.*, 1993, **97**, 432–439.

169 D. Chen, S. Sharma, I. Filimonov and J. Dumesic, *Catal. Lett.*, 1992, **12**, 201–211.

170 W. Trisunaryanti, K. Wijaya, I. Kartini, S. Purwono, A. Mara and A. Budiyansah, *Commun. Sci. Technol.*, 2023, **8**, 226–234.

171 M. Kumar, Z. J. Berkson, R. J. Clark, Y. Shen, N. A. Prisco, Q. Zheng, Z. Zeng, H. Zheng, L. B. McCusker and J. C. Palmer, *J. Am. Chem. Soc.*, 2019, **141**, 20155–20165.

172 N. Chaihad, S. Karnjanakom, A. Abudula and G. Guan, *Resour. Chem. Mater.*, 2022, **1**, 167–183.

173 W. Luo, W. Cao, P. C. Bruijnincx, L. Lin, A. Wang and T. Zhang, *Green Chem.*, 2019, **21**, 3744–3768.

174 V. G. Matveeva and L. M. Bronstein, *Nanomaterials*, 2023, **13**, 2274.

175 Y.-L. Ding, H.-Q. Wang, M. Xiang, P. Yu, R.-Q. Li and Q.-P. Ke, *Front. Chem.*, 2020, **8**, 790.

176 H. Lee, H. Kim, M. J. Yu, C. H. Ko, J.-K. Jeon, J. Jae, S. H. Park, S.-C. Jung and Y.-K. Park, *Sci. Rep.*, 2016, **6**, 28765.

177 Y. Wang, X. Yuan, J. Liu and X. Jia, *ChemPlusChem*, 2024, **89**, e202300399.

178 R. Cuevas-García, J. Téllez-Romero, J. Ramírez, P. Sarabia-Bañuelos, I. Puente-Lee, C. Salcedo-Luna, S. Hernández-González and V. Nolasco-Arizmendi, *Catal. Today*, 2021, **360**, 63–71.

179 L. Hu, X.-Y. Wei and Z.-M. Zong, *J. Energy Inst.*, 2021, **97**, 48–57.

180 D. He, D. Chen, H. Hao, J. Yu, J. Liu, J. Lu, G. Wan, S. He, K. Li and Y. Luo, *Chem. Eng. J.*, 2017, **317**, 60–69.

181 M. A. Sanchez-Castillo, R. J. Madon and J. A. Dumesic, *J. Phys. Chem. B*, 2005, **109**, 2164–2175.

182 H.-T. Vu, M. Goepel and R. Gläser, *RSC Adv.*, 2021, **11**, 5568–5579.

183 E. F. Sousa-Aguiar, F. E. Trigueiro and F. M. Z. Zotin, *Catal. Today*, 2013, **218**, 115–122.

184 R. Simancas, A. Chokkalingam, S. P. Elangovan, Z. Liu, T. Sano, K. Iyoki, T. Wakihara and T. Okubo, *Chem. Sci.*, 2021, **12**, 7677–7695.

185 J. N. Louwen, S. Simko, K. Stanciakova, R. E. Bulo, B. M. Weckhuysen and E. T. Vogt, *J. Phys. Chem. C*, 2020, **124**, 4626–4636.

186 Y. Xi, Y. Chu, Q. Wang, N. Feng, J. Xu and F. Deng, *J. Phys. Chem. C*, 2025, **129**, 14020–14032.

187 A. Zornes, O. R. Das, N. B. Abdul Rahman, J. Crouch, S. Crossley, B. Wang, W. Alvarez, M. J. Wulfers, D. E. Resasco and J. L. White, *J. Phys. Chem. C*, 2025, **129**, 8545–8555.